DUAL-LEVEL AFFINITY INDUCED EMBEDDING-FREE MULTI-VIEW CLUSTERING WITH JOINT-ALIGNMENT

Anonymous authors
Paper under double-blind review

ABSTRACT

Despite remarkable progress, there still exist several limitations in current multi-view clustering (MVC) techniques. Specially, they generally focus only on the affinity relationship between anchors and samples, while overlooking that between anchors. Moreover, due to the lack of data labels, the cluster order is inconsistent across views and accordingly anchors encounter misalignment issue, which will confuse the graph structure and disorganize cluster representation. Even worse, it typically brings variance during forming embedding, degenerating the stability of clustering results. In response to these concerns, in the paper we propose a MVC approach named DLA-EF-JA. Concretely, we explicitly exploit the geometric properties between anchors via self-expression learning skill, and utilize topology learning strategy to feed captured anchor-anchor features into anchor-sample graph so as to explore the manifold structure hidden within samples more adequately. To reduce the misalignment risk, we introduce a permutation mechanism for each view to jointly rearrange anchors according to respective view characteristics. Besides not involving selecting the baseline view, it also can coordinate with anchors in the unified framework and thereby facilitate the learning of anchors. Further, rather than forming embedding and then performing spectral partitioning, based on the criterion that samples and clusters should be hard assignment, we manage to construct the cluster labels directly from original samples using the binary strategy, not only preserving the data diversity but avoiding variance. Experiments on multiple publicly available datasets confirm the effectiveness of our DLA-EF-JA.

1 INTRODUCTION

In recent years, multi-view clustering (MVC) is becoming a research hotspot because of its ability to effectively mine potential patterns hidden in heterogeneous data, and is widespreadly deployed in various fields such as drug design and finance analysis (Xu et al., 2024; Chen et al., 2023b; Xia et al., 2022a; Wang et al., 2023b; Wen et al., 2024a; Wang et al., 2022b; Wen et al., 2023b; Xu et al., 2023b). As a powerful tool in MVC, anchor technique is commonly utilized to filter noise points and decrease the computing overhead (Li et al., 2023; He et al., 2023; Li et al., 2024b). It first selects a small number of significant samples to represent overall samples, and then replaces the sample-sample affinity relationship by building up the anchor-sample relationship (Zhao et al., 2024; Yang et al., 2022; Nie et al., 2024b). Following this line, a series of prominent works have been successively proposed. For instance, Kang et al. (2020b) regard the centroids generated by k-means on respective view as anchors and merge multiple graphs by splicing their left singular vectors. Xia et al. (2022b) first project samples to perform de-correlation and then select anchors in projection space according to the sample variance. Wang et al. (2022a) design a hierarchical k-means model to output anchors and construct sparse similarity using the learned bipartite graph. Huang et al. (2023) leverage three diversity levels in neighbors to construct anchors and generate graph directly in the early-stage fusion.

Although generating pleasing clustering results from various aspects, current methods usually focus only on the anchor-sample affinity, and fail to take into account the anchor-anchor characteristics. This is not reasonable since between anchors, there generally exist informative geometric features. Overlooking them will not be conductive to constructing discriminative anchors and extracting the intrinsic similarity among samples. Additionally, due to the fact that clustering tasks do not involve any data labels, anchors could be misaligned across views, leading to the graph structure becoming chaotic. Wang et al. (2022c) provide an alignment scheme from the perspectives of feature and structure matching, nevertheless, it requires to select the baseline view. Also, the anchor generation, the anchor transformation, and the graph construction are separated from each other. These limitations hinder the interaction of view information across different levels and accordingly weaken the distinctiveness of anchors. Furthermore, the clustering procedure adopted by current approaches is to first form embedding and then conduct spectral partitioning on it, which causes the generated clustering results containing non-zero variance, degrading the stability and interpretability.

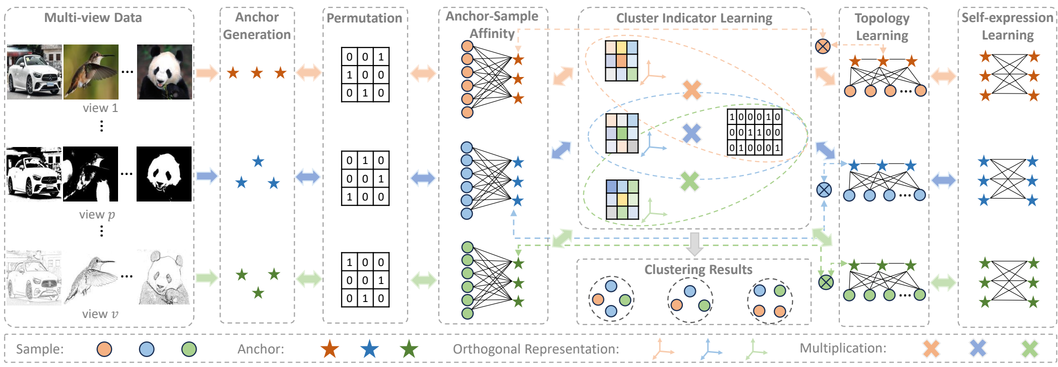

Figure 1: The devised DLA-EF-JA framework. It explicitly extracts the geometric characteristics of anchor-anchor via self-expression learning, and delivers them into the topology learning of anchor-sample to exploit the manifold structure among samples. It introduces a learnable permutation model for each view to alleviate the anchor misalignment. Instead of constructing embedding, it directly learns the cluster indicators via binary learning to avoid introducing variance. These three sub-parts are all jointly optimized within an unified framework so as to move towards mutual reinforcement.

With these concerns in minds, we design a MVC method termed DLA-EF-JA in this paper, and its framework is presented in Fig. 1. To be specific, we introduce self-expression learning mechanism to explore the geometric characteristics between anchors, and integrate them into the topology learning of anchor-sample graph so as to characterize the manifold structure inside samples more sufficiently. Then, we associate each view with a permutation model, which is learnable and works jointly with the anchor generation, to rearrange anchors in their original dimension space according to view-specific features. Owing to the joint-optimization mechanism in the unified framework, consequently, it does not involve the selection of baseline view. Further, to eliminate variance, based on the criterion that one sample should belong to only one cluster, we avoid the formation of embedding and choose to directly generate cluster indicators from original samples. When the sample belongs to its cluster, we manage to optimize its indicator as 1 and otherwise 0. In addition to well preserving the data diversity, this paradigm also can skip the spectral partitioning stage and thereby alleviate the computing burden. The cluster indicator matrix is shared for all views, which bridges all anchors, permutations and views. Not only does it play an important role in gathering multi-view information at the cluster-label level, but provides consensus structure for anchors on different views to force them rearranging towards correct-matching direction. Subsequently, we give a six-step updating scheme with linear complexity to optimize the resultant objective loss. Experiments on various benchmark datasets demonstrate that DLA-EF-JA is effective in grouping multi-view data and owns competitive strengths against multiple classical MVC approaches. For more clarity, we summary the contributions of this work as below,

1. We explicitly take into account the geometric features between anchors, and successfully integrate them into the anchor-sample graph through topology learning to exploit the manifold characteristics hidden within samples more fully for better clustering.

2. We devise a joint-alignment mechanism that not only eliminates the need for selecting the baseline view but also coordinates well with the generation of anchors.

3. We avoid the formation of embedding by directly learning cluster indicators using a binary strategy, which effectively clears the variance in clustering results, accordingly highlighting the stability.

4. We provide a six-step optimization scheme with linear complexity for the loss function. Experiments validate the effectiveness of our proposed method from multiple aspects.

2 Related Work

Based on the fact that each view data typically owns self-unique features and consequently can compensate for the limitations of other views, multi-view clustering aims at integrating information from diverse views to obtain more comprehensive and accurate data representation, thereby achieving superior clustering effect than single-view counterparts (Xu et al., 2023a; Wang et al., 2024; Huang et al., 2024b; Wen et al., 2023a; Zhang et al., 2019; Tang & Liu, 2022; Fang et al., 2023; Wang et al., 2023a). Anchor technology is recently introduced into multi-view clustering to increase the computing efficiency (Shi et al., 2021; Chen et al., 2024). It is intended to replace the full graph with a small-sized anchor graph by utilizing some discriminative landmarks. Specially, given a multi-view dataset $\{\mathbf{X}_p \in \mathbb{R}^{d_p \times n}\}_{p=1}^{v}$ where d_p, n and v denote the dimension of data, the number of samples and the number of views respectively, anchor based multi-view clustering can be formulated as

$$\min_{\{\mathbf{Z}_p^\top \mathbf{1}=\mathbf{1},\mathbf{Z}_p\geq 0\}_{p=1}^{v},\mathbf{Z}^\top\mathbf{1}=\mathbf{1},\mathbf{Z}\geq 0} \sum_{p=1}^{v} \left\|\mathbf{X}_p - \mathbf{A}_p\mathbf{Z}_p\right\|_F^2 + \eta \left\|\mathbf{Z}_p\right\|_F^2 + \gamma \left\|\mathbf{Z}_p - \mathbf{Z}\right\|_F^2, \tag{1}$$

where $\mathbf{A}_p \in \mathbb{R}^{d_p \times m}$, $\mathbf{Z}_p \in \mathbb{R}^{m \times n}$, η and γ denote the anchor matrix, anchor graph and regularization hyper-parameters, respectively. The fusion graph $\mathbf{Z} \in \mathbf{R}^{m\times n}$ aims at gathering the information from different views at the graph level. The non-negative constraints and column sum constraints guarantee the learned graph to satisfy the similarity requirements. After obtaining $\mathbf{Z}$, the cluster labels can be received by first constructing embedding on the fusion graph $\mathbf{Z}$ and then conducting spectral partitioning operation on the embedding.

Noticed that the final clustering results are heavily dependent on the quality of $\mathbf{Z}_p$ while $\mathbf{Z}_p$ is related to anchor matrix $\mathbf{A}_p$, consequently, many works focus on the generation way of anchors. For example, Chen et al. (2023c) utilize tensor learning to investigate the low-rankness within views and employ a dynamic anchor learning strategy to explore that between views. Yan et al. (2022) integrate anchor learning and feature learning together, and learn to generate anchors separately. Given the fact that similar samples typically lie in the same cluster and have homologous characteristics, Li et al. (2022a) devise an alternative sampling scheme, which is independent of initialization, to generate anchors. Liu et al. (2024) narrow the distributions of anchors by leveraging the correlation information between views to enhance their distinction. These methods successfully construct representative anchors from different perspectives, nevertheless, they generally pay only attention to the relationship between anchors and samples when constructing anchor graph, while overlooking the influence of geometric characteristics inside anchors. This could bring about the loss of some informative features. Anchors on different views also could be misaligned due to the unsupervised property of data, leading to the confusion of graph structure (Wang et al., 2022c). Moreover, the clustering results outputted by current methods usually contain variance when partitioning the embedding, which exacerbates the instability (Zhang et al., 2020a; Zeng et al., 2024; Chen et al., 2023a). In next section, we will elaborate in detail on the principles of our devised DLA-EF-JA approach to alleviate these issues.

3 Methodology

To explore the geometric properties between anchors, inspired by subspace reconstruction (Zhang et al., 2020b; Xia et al., 2022d), we introduce self-expression learning for anchors. To be specific, we utilize the paradigm $\left\|\mathbf{A}_p - \mathbf{A}_p\mathbf{S}_p\right\|_F^2$ to explicitly extract the global structure between anchors. Especially, due to $\mathbf{S}_p \in \mathbf{R}^{m\times m}$ where m is the number of anchors, solving $\mathbf{S}_p$ will take $\mathcal{O}(m^3)$ computing overhead, which is almost ignorable against $\mathcal{O}(m^2 n)$ that solving $\mathbf{Z}_p$ takes since m is far less than n. Then, to integrate the characteristics of anchor-anchor into anchor-sample so as to exploit the manifold features inside samples, we adopt the idea of point-point guidance to adjust the anchor graph. That is, we utilize the element $[\mathbf{S}_p]_{i,j}$ to guide $[\mathbf{Z}_p]_{i,t}$ and $[\mathbf{Z}_p]_{j,t}, i, j = 1, \cdots, m, t = 1, \cdots n$, which can be formulated as $\sum_{i,j=1}^{m} \left\|[\mathbf{Z}_p]_{i,:} - [\mathbf{Z}_p]_{j,:}\right\|_2^2 [\mathbf{S}_p]_{i,j}$ and aims at restricting similar features to maintain the consistency. At this point, the MVC framework can be formulated as

$$\begin{aligned} \min_{\{\mathbf{Z}_p,\mathbf{S}_p\}_{p=1}^{v}} & \sum_{p=1}^{v} \left\|\mathbf{X}_p - \mathbf{A}_p\mathbf{Z}_p\right\|_F^2 + \lambda \left\|\mathbf{A}_p - \mathbf{A}_p\mathbf{S}_p\right\|_F^2 + \beta \sum_{i,j=1}^{m} \left\|[\mathbf{Z}_p]_{i,:} - [\mathbf{Z}_p]_{j,:}\right\|_2^2 [\mathbf{S}_p]_{i,j} \\ & \text{s.t. } \mathbf{Z}_p^\top \mathbf{1} = \mathbf{1}, \mathbf{Z}_p \geq 0, \mathbf{S}_p^\top \mathbf{1} = \mathbf{1}, \mathbf{S}_p \geq 0, \sum_{i=1}^{m} [\mathbf{S}_p]_{i,i} = 0. \end{aligned} \tag{2}$$

Subsequently, to eliminate the anchor misalignment issue, one straightforward idea is to compute the space similarity between anchor sets and then match anchors according to their distance. However, multi-view data generally has various dimensions, and accordingly anchors on different views also have various dimensions. It is typically difficult to directly compute the distance between anchor sets with diverse dimensions. Although one can project all anchors into a common space to make them have the same dimension, it can not guarantee the distance similarity after projecting to be consistent with that before projecting. Additionally, determining the appropriate projection dimension needs heuristic searching. The projecting operation also could lead to heavy information loss. Consequently, these strategies are not that sensible. To get rid of this dilemma, considering that the nature of anchor misalignment is that the order of anchors on different views is not identical, we can alleviate the misalignment issue by rearranging anchors. In particular, we associate each view with a learnable permutation matrix $\mathbf{T}_p \in \mathbb{R}^{m\times m}$ to flexibly transform anchors according to the characteristics of respective view, i.e., $\|\mathbf{X}_p - \mathbf{A}_p\mathbf{T}_p\mathbf{Z}_p\|_F^2$. The subsequent issue is how to make anchors rearrange towards the correct matching direction. Next, we solve it and the variance issue concurrently.

Due to variance arising from the construction of embedding, we avoid forming embedding, and choose to directly learn the cluster indicators. We factorize the anchor graph as a basic coefficient matrix and a consensus matrix, and utilize binary learning to optimize the consensus matrix. This not only makes the consensus matrix successfully represent the cluster indicators, but also provides a common structure for anchors on all views, inducing them rearranging towards the common structure. Further, since views typically own different levels of importance, we introduce a weighting variable for each view to automatically measure its contributions. Therefore, our DLA-EF-JA is devised as

$$\begin{gathered}\min_{\boldsymbol{\Omega}} \sum_{p=1}^{v} \boldsymbol{\alpha}_p^2 \left\|\mathbf{X}_p - \mathbf{A}_p\mathbf{T}_p\mathbf{B}_p\mathbf{C}\right\|_F^2 + \lambda \left\|\mathbf{A}_p\mathbf{T}_p - \mathbf{A}_p\mathbf{T}_p\mathbf{S}_p\right\|_F^2 + \beta\, \mathrm{Tr}(\mathbf{B}_p^\top \mathbf{L_s}\mathbf{B}_p\mathbf{C}\mathbf{C}^\top) \\ \text{s.t. } \boldsymbol{\alpha}^\top\mathbf{1} = 1, \boldsymbol{\alpha} \geq 0, \mathbf{B}_p^\top\mathbf{B}_p = \mathbf{I}_k, \mathbf{T}_p^\top\mathbf{1} = \mathbf{1}, \mathbf{T}_p\mathbf{1} = \mathbf{1}, \mathbf{T}_p \in \{0,1\}^{m\times m}, \\ \sum_{i=1}^{k} \mathbf{C}_{i,j} = 1, j = 1,2,\ldots,n, \mathbf{C} \in \{0,1\}^{k\times n}, \mathbf{S}_p^\top\mathbf{1} = \mathbf{1}, \mathbf{S}_p \geq 0, \sum_{i=1}^{m}[\mathbf{S}_p]_{i,i} = 0,\end{gathered} \tag{3}$$

where $\boldsymbol{\Omega} = \{\mathbf{A}_p \in \mathbb{R}^{d_p\times m}, \mathbf{B}_p \in \mathbb{R}^{m\times k}, \mathbf{S}_p \in \mathbb{R}^{m\times m}, \mathbf{T}_p \in \mathbb{R}^{m\times m}, \boldsymbol{\alpha} \in \mathbb{R}^{v\times 1}, \mathbf{C} \in \mathbb{R}^{k\times n}; p = 1, \cdots, v\}$. The second term aims at capturing the characteristics between anchors. The third term is the matrix form of point-point guidance, and aims at delivering the characteristics of anchor-anchor into anchor-sample of the first term, where $\mathbf{L_s} \in \mathbb{R}^{m\times m} = \mathbf{D}_p - \mathbf{S}_p, \mathbf{D}_p = diag\{\sum_{j=1}^{m}[\mathbf{S}_p]_{i,j} \mid, i = 1, \cdots, m\}$. This embedding-free model directly output discrete clustering results via the consensus cluster indicator matrix $\mathbf{C}$. The vector $\boldsymbol{\alpha}$ plays a role in adjusting the importance between views.

4 Solver

We adopt the alternating optimization scheme to minimize the loss function Eq. (3).

Update $\mathbf{A}_p$: The optimization w.r.t $\mathbf{A}_p$ in Eq. (3) can be written as

$$\min_{\mathbf{A}_p} \boldsymbol{\alpha}_p^2 \left\|\mathbf{X}_p - \mathbf{A}_p\mathbf{T}_p\mathbf{B}_p\mathbf{C}\right\|_F^2 + \lambda \left\|\mathbf{A}_p\mathbf{T}_p - \mathbf{A}_p\mathbf{T}_p\mathbf{S}_p\right\|_F^2. \tag{4}$$

By using the derivative equal to zero, we can obtain

$$\mathbf{A}_p = \boldsymbol{\alpha}_v^2\mathbf{X}_p\mathbf{E}_p^\top \left(\boldsymbol{\alpha}_v^2\mathbf{E}_p\mathbf{E}_p^\top + \lambda\mathbf{F}_p\mathbf{F}_p^\top\right)^{-1}, \tag{5}$$

where $\mathbf{E}_p \in \mathbb{R}^{m\times n} = \mathbf{T}_p\mathbf{B}_p\mathbf{C}, \mathbf{F}_p \in \mathbb{R}^{m\times m} = \mathbf{T}_p - \mathbf{T}_p\mathbf{S}_p$.

Update $\mathbf{T}_p$: The optimization w.r.t $\mathbf{T}_p$ in Eq. (3) can be written as

$$\begin{gathered}\min_{\mathbf{T}_p} \boldsymbol{\alpha}_p^2 \left\|\mathbf{X}_p - \mathbf{A}_p\mathbf{T}_p\mathbf{B}_p\mathbf{C}\right\|_F^2 + \lambda \left\|\mathbf{A}_p\mathbf{T}_p - \mathbf{A}_p\mathbf{T}_p\mathbf{S}_p\right\|_F^2 \\ \text{s.t. } \mathbf{T}_p^\top\mathbf{1} = \mathbf{1}, \mathbf{T}_p\mathbf{1} = \mathbf{1}, \mathbf{T}_p \in \{0,1\}^{m\times m}.\end{gathered} \tag{6}$$

Expanding the objective by trace operation, Eq. (6) can be further equivalently transformed as

$$\begin{gathered}\min_{\mathbf{T}_p} \mathrm{Tr}\left(\mathbf{T}_p^\top\mathbf{G}_p\mathbf{T}_p\left(\lambda\mathbf{H}_p + \boldsymbol{\alpha}_p^2\mathbf{M}_p - 2\lambda\mathbf{S}_p^\top\right) - 2\boldsymbol{\alpha}_p^2\mathbf{T}_p^\top\mathbf{J}_p\right) \\ \text{s.t. } \mathbf{T}_p^\top\mathbf{1} = \mathbf{1}, \mathbf{T}_p\mathbf{1} = \mathbf{1}, \mathbf{T}_p \in \{0,1\}^{m\times m},\end{gathered} \tag{7}$$

where $\mathbf{G}_p \in \mathbb{R}^{m\times m} = \mathbf{A}_p^\top \mathbf{A}_p$, $\mathbf{H}_p \in \mathbb{R}^{m\times m} = \mathbf{S}_p \mathbf{S}_p^\top$, $\mathbf{M}_p \in \mathbb{R}^{m\times m} = \mathbf{B}_p \mathbf{C}\mathbf{C}^\top \mathbf{B}_p^\top$ and $\mathbf{J}_p \in \mathbb{R}^{m\times m} = \mathbf{A}_p^\top \mathbf{X}_p \mathbf{C}^\top \mathbf{B}_p^\top$. Given the characteristics of feasible region, we can obtain the optimal $\mathbf{T}_p$ via traversal searching on the one-hot vectors $\{\mathbf{e}_i\}_{i=1}^m$.

Update $\mathbf{B}_p$: The optimization w.r.t $\mathbf{B}_p$ in Eq. (3) can be written as

$$\min_{\mathbf{B}_p} \operatorname{Tr}\left(\mathbf{B}_p^\top \left(\beta \mathbf{L_s} + \boldsymbol{\alpha}_p^2 \mathbf{Q}_p\right) \mathbf{B}_p \mathbf{C}\mathbf{C}^\top - 2\boldsymbol{\alpha}_p^2 \mathbf{C}\mathbf{X}_p^\top \mathbf{A}_p \mathbf{T}_p \mathbf{B}_p\right) \text{ s.t. } \mathbf{B}_p^\top \mathbf{B}_p = \mathbf{I}_k, \tag{8}$$

where $\mathbf{Q}_p \in \mathbb{R}^{m\times m} = \mathbf{T}_p^\top \mathbf{A}_p^\top \mathbf{A}_p \mathbf{T}_p$. Then, we split the feasible region into $[\mathbf{B}_p]_{:,i}^\top [\mathbf{B}_p]_{:,i} = 1$ and $[\mathbf{B}_p]_{:,i}^\top [\mathbf{B}_p]_{:,j} = 0$, $i \neq j$. Further, combined with the fact that $\mathbf{C}\mathbf{C}^\top$ is a diagonal matrix, Eq. (8) can be equivalently transformed as

$$\begin{gathered}\min_{[\mathbf{B}_p]_{:,j}} [\mathbf{B}_p]_{:,j}^\top \sum_{i=1}^n \mathbf{C}_{j,i} \left(\beta \mathbf{L_s} + \boldsymbol{\alpha}_p^2 \mathbf{Q}_p\right) [\mathbf{B}_p]_{:,j} + \left[-2\boldsymbol{\alpha}_p^2 \mathbf{C}\mathbf{X}_p^\top \mathbf{A}_p \mathbf{T}_p\right]_{j,:} [\mathbf{B}_p]_{:,j} \\ \text{s.t. } [\mathbf{B}_p]_{:,j}^\top \mathbf{I}_{m\times m} [\mathbf{B}_p]_{:,j} - 1 = 0, \\ \left[[\mathbf{B}_p]_{:,1}, [\mathbf{B}_p]_{:,2}, \cdots, [\mathbf{B}_p]_{:,j-1}, [\mathbf{B}_p]_{:,j+1}, \cdots, [\mathbf{B}_p]_{:,k}\right]^\top [\mathbf{B}_p]_{:,j} = \mathbf{0}_{(k-1)\times 1}.\end{gathered} \tag{9}$$

It is a quadratically constrained quadratic programming and can be solved by current software.

Update $\mathbf{S}_p$: The optimization w.r.t $\mathbf{S}_p$ in Eq. (3) can be written as

$$\min_{\mathbf{S}_p} \operatorname{Tr}\left(\mathbf{S}_p^\top \mathbf{Q}_p \mathbf{S}_p + 2\left(-\mathbf{Q}_p - \frac{\beta}{2\lambda}\mathbf{M}_p\right)\mathbf{S}_p\right) \text{ s.t. } \mathbf{S}_p^\top \mathbf{1} = \mathbf{1}, \mathbf{S}_p \geq 0, \sum_{i=1}^m [\mathbf{S}_p]_{i,i} = 0. \tag{10}$$

Noticed that the constraints can be equivalently transformed as $\boldsymbol{\Psi} = \left\{[\mathbf{S}_p]_{:,j}^\top \mathbf{1} = 1, 0 \leq [\mathbf{S}_p]_{:,j}, \mathbf{e}_j^\top [\mathbf{S}_p]_{:,j} = 0, j = 1, 2, \cdots, m\right\}$, and therefore Eq. (10) is further converted as

$$\min_{\boldsymbol{\Psi}} [\mathbf{S}_p]_{:,j}^\top \mathbf{Q}_p [\mathbf{S}_p]_{:,j} + 2\left(-\mathbf{Q}_p - \frac{\beta}{2\lambda}\mathbf{M}_p\right)_{j,:} [\mathbf{S}_p]_{:,j}. \tag{11}$$

It is a quadratic programming and can be easily solved.

Update $\mathbf{C}$: The optimization w.r.t $\mathbf{C}$ in Eq. (3) can be written as

$$\min_{\mathbf{C}} \operatorname{Tr}\left(\mathbf{C}^\top \mathbf{W}\mathbf{C} - \mathbf{Z}\mathbf{C}\right) \text{ s.t. } \sum_{i=1}^k \mathbf{C}_{i,j} = 1, j = 1, 2, \ldots, n, \mathbf{C} \in \{0,1\}^{k\times n}, \tag{12}$$

where $\mathbf{W} \in \mathbb{R}^{k\times k} = \sum_{p=1}^v \boldsymbol{\alpha}_p^2 \mathbf{B}_p^\top \mathbf{T}_p^\top \mathbf{A}_p^\top \mathbf{A}_p \mathbf{T}_p \mathbf{B}_p + \beta \mathbf{B}_p^\top \mathbf{L_s} \mathbf{B}_p$, $\mathbf{Z} \in \mathbb{R}^{n\times k} = 2\sum_{p=1}^v \boldsymbol{\alpha}_p^2 \mathbf{X}_p^\top \mathbf{A}_p \mathbf{T}_p \mathbf{B}_p$. The constraints indicate that there is only one non-zero element in each column of $\mathbf{C}$, and thus we can solve $\mathbf{C}$ column by column. Eq. (12) can be further transformed as

$$\min_{\mathbf{C}_{:,j}} \mathbf{C}_{:,j}^\top \mathbf{W}\mathbf{C}_{:,j} - \mathbf{Z}_{j,:}\mathbf{C}_{:,j} \text{ s.t. } \sum_{i=1}^k \mathbf{C}_{i,j} = 1, \mathbf{C}_{:,j} \in \{0,1\}^{k\times 1}. \tag{13}$$

The item $\mathbf{C}_{:,j}^\top \mathbf{W}\mathbf{C}_{:,j}$ means that it takes a certain diagonal element of $\mathbf{W}$, and $\mathbf{Z}_{j,:}\mathbf{C}_{:,j}$ takes a certain element of $\mathbf{Z}_{j,:}$. Therefore, we can determine the corresponding index of minimum by $l^* = \arg\min_l \mathbf{W}_{l,l} - \mathbf{Z}_{j,l}$, $l = 1, 2, \cdots, k$. Then, the value of $\mathbf{C}_{:,j}$ can be obtained by

$$\mathbf{C}_{i,j} = \begin{cases} 1, & i = l^*, \\ 0, & i \neq l^*, i = 1, 2, \cdots, k. \end{cases} \tag{14}$$

Update $\boldsymbol{\alpha}$: The optimization w.r.t $\boldsymbol{\alpha}$ in Eq. (3) can be written as

$$\min_{\boldsymbol{\alpha}} \sum_{p=1}^v \boldsymbol{\alpha}_p^2 \left\|\mathbf{X}_p - \mathbf{A}_p \mathbf{T}_p \mathbf{B}_p \mathbf{C}\right\|_F^2 \text{ s.t. } \boldsymbol{\alpha}^\top \mathbf{1} = 1, \boldsymbol{\alpha} \geq 0. \tag{15}$$

Since the item $\frac{1}{b_p} = \left\|\mathbf{X}_p - \mathbf{A}_p \mathbf{T}_p \mathbf{B}_p \mathbf{C}\right\|_F^2$ is a constant for $\boldsymbol{\alpha}$, the optimal $\boldsymbol{\alpha}$ can be determined via Cauchy inequality. Thus, we have

$$\boldsymbol{\alpha}_p = \frac{b_p}{\sum_{p=1}^v b_p}. \tag{16}$$

Algorithm 1 summarizes the overall pipeline of our DLA-EF-JA.

5 Complexity Analysis

Space complexity The space complexity of DLA-EF-JA is mainly from optimization variables $\mathbf{A}_p$, $\mathbf{T}_p$, $\mathbf{B}_p$, $\mathbf{S}_p$, $\mathbf{C}$ and $\boldsymbol{\alpha}$, $p = 1, 2, \cdots, v$. According to the fact that $\mathbf{A}_p \in \mathbb{R}^{d_p \times m}$, $\mathbf{T}_p \in \mathbb{R}^{m \times m}$, $\mathbf{B}_p \in \mathbb{R}^{m \times k}$, $\mathbf{S}_p \in \mathbb{R}^{m \times m}$, $\mathbf{C} \in \mathbb{R}^{k \times n}$ and $\boldsymbol{\alpha} \in \mathbb{R}^{v \times 1}$, we have that storing them will require $\mathcal{O}(d_p m)$, $\mathcal{O}(m^2)$, $\mathcal{O}(mk)$, $\mathcal{O}(m^2)$, $\mathcal{O}(nk)$ and $\mathcal{O}(1)$ memory overhead, respectively. Thus, storing all optimization variables will take $\mathcal{O}(dm + m^2 v + mkv + nk)$ overhead where d represents the data dimension sum of all views and is independent of the sample size n. Further, since the number of anchors m is generally greater than or equal to the number of clusters k, we have $m^2 v \geq mkv$. Besides, considering that m is generally much smaller than n and is also independent of n, we have that the space complexity of the proposed DLA-EF-JA is $\mathcal{O}(nk)$, which is linearly related to the sample size n.

Time complexity The time complexity of DLA-EF-JA is mainly from the updating of all optimization variables. When updating $\mathbf{A}_p$, constructing $\mathbf{E}_p$ and $\mathbf{F}_p$ will take $\mathcal{O}(m^2 k + mkn)$ and $\mathcal{O}(m^3)$ respectively. Constructing the item $\boldsymbol{\alpha}_v^2 \mathbf{E}_p \mathbf{E}_p^\top + \lambda \mathbf{F}_p \mathbf{F}_p^\top$ and solving its inverse will take $\mathcal{O}(m^2 n + m^3)$ and $\mathcal{O}(m^3)$ respectively. Thus, updating $\mathbf{A}_p$ will take $\mathcal{O}(m^2 k + mkn + m^2 n + m^3 + d_p nm + d_p m^2)$. When updating $\mathbf{T}_p$, constructing $\mathbf{G}_p$, $\mathbf{H}_p$, $\mathbf{M}_p$ and $\mathbf{J}_p$ will take $\mathcal{O}(d_p m^2)$, $\mathcal{O}(m^3)$, $\mathcal{O}(mkn + m^2 n)$ and $\mathcal{O}(d_p mn + mnk + m^2 k)$, respectively. Traversal searching on one-hot vectors will take $\mathcal{O}(m!)$. Thus, updating $\mathbf{T}_p$ will take $\mathcal{O}(d_p m^2 + d_p mn + m^3 + mkn + m^2 n + m!)$. When updating $\mathbf{B}_p$, constructing $\mathbf{Q}_p$ and the item $\mathbf{C}\mathbf{X}_p^\top \mathbf{A}_p \mathbf{T}_p \mathbf{B}_p$ will take $\mathcal{O}(d_p m^2)$ and $\mathcal{O}(knd_p + kd_p m + km^2 + k^2 m)$, respectively. Performing quadratically constrained quadratic programming will take $\mathcal{O}(m^3 k)$. Thus, updating $\mathbf{B}_p$ will take $\mathcal{O}(d_p m^2 + knd_p + k^2 m + m^3 k)$. When updating $\mathbf{S}_p$, due to the construction of $\mathbf{Q}_p$ and $\mathbf{M}_p$ having been completed, it only involves the performing of quadratic programming, which will take $\mathcal{O}(m^3)$. When updating $\mathbf{C}$, constructing $\mathbf{W}$ and $\mathbf{Z}$ will take $\mathcal{O}(d_p m^2 + d_p mk + d_p k^2 + km^2 + k^2 m)$ and $\mathcal{O}(nd_p m + nm^2 + nmk)$, respectively. Since the value of $\mathbf{C}$ can be determined by comparing the diagonal element of $\mathbf{W}$ and the row of $\mathbf{Z}$, updating $\mathbf{C}$ will take $\mathcal{O}(d_p mk + d_p k^2 + km^2 + k^2 m + nd_p m + nm^2 + nmk)$. When updating $\boldsymbol{\alpha}$, constructing b_p will take $\mathcal{O}(d_p m^2 + d_p mk + d_p kn)$. The value of $\boldsymbol{\alpha}$ can be determined by Cauchy inequality, and thus updating $\boldsymbol{\alpha}$ will $\mathcal{O}(d_p m^2 + d_p mk + d_p kn)$. Based on these, we have that updating all $\mathbf{A}_p$, $\mathbf{T}_p$, $\mathbf{B}_p$, $\mathbf{S}_p$, $\mathbf{C}$ and $\boldsymbol{\alpha}$ will take $\mathcal{O}(mknv + m^2 nv + dnm + dm^2 + m!v + m^3 kv + knd + k^2 mv + dk^2)$. Besides, considering that m is usually greater than or equal to k, d_p is independent of n, n is largely greater than m, we can obtain that updating all variables will take $\mathcal{O}(m^2 nv + dnm + m!v + m^3 kv)$, which is also linearly related to the sample size n.

6 Experiments

6.1 Experimental Setting

Datasets We evaluate the algorithm performance on the following 7 datasets: DERMATO, CALTE7, Cora, REU7200, Reuters, CIF10Tra4, FasMNI4V.

Baselines We choose the following 20 classical MVC methods as the baselines to demonstrate the effectiveness of DLA-EF-JA: FMR (Li et al., 2019), PMSC (Kang et al., 2020a), AMGL (Nie et al., 2016), MSCIAS (Wang et al., 2019), MVSC (Gao et al., 2015), MLRSSC (Brbić & Kopriva, 2018), MPAC (Kang et al., 2019), MCLES (Chen et al., 2020), FMCNOF (Yang et al., 2021), ADA-GAE (Li et al., 2022b), PFSC (Lv et al., 2021), SFMC (Li et al., 2022a), MSGL(Kang et al., 2022), FPMVS (Wang et al., 2022d), MFLVC (Xu et al., 2022), UOMVSC (Tang et al., 2023), PGSC(Wu et al., 2023), OrthNTF(Li et al., 2024c), FMVACC(Wang et al., 2022c), FASTMI(Huang et al., 2023).

Algorithm 1 Our proposed DLA-EF-JA

Input: Multi-view data $\{\mathbf{X}_p\}_{p=1}^v$, hyper-parameters λ and β.
Output: Discrete cluster indicator matrix $\mathbf{C}$.
Initialize: $\{\mathbf{A}_p, \mathbf{T}_p, \mathbf{B}_p, \mathbf{S}_p\}_{p=1}^v$, $\mathbf{C}$, $\boldsymbol{\alpha}$.

```
repeat
    Update A_p via Eq. (5)
    Update T_p via Eq. (7)
    Update B_p via Eq. (9)
    Update S_p via Eq. (11)
    Update C via Eq. (14)
    Update α_p via Eq. (16)
until convergent
```

Parameter Setup We search the hyper-parameters λ and β in $[10^{-1}, 10^0, 10^1, 10^2, 10^3]$ and $[2^{-4}, 2^{-2}, 2^0, 2^2, 2^4]$ respectively. For all competitors, we download their source code and tune the parameters according to their provided guidelines. Three popular metrics are used to measure the clustering results. For fairness, we run 20 times and calculate the mean and variance of results.

Table 1: Clustering result comparison (mean±std). Red and blue denote the top 2 results.

Dataset	DERMATO	CALTE7	Cora	REU7200	Reuters	CIF10Tra4	FasMNI4V
			NMI(%)				
FMR (Li et al., 2019)	79.18(±3.85)	44.81(±0.93)	20.63(±1.21)	-	-	-	-
PMSC (Kang et al., 2020a)	86.14(±4.84)	44.93(±0.81)	6.12(±0.67)	4.02(±0.55)	-	-	-
AMGL (Nie et al., 2016)	4.56(±0.72)	44.95(±2.07)	2.74(±0.36)	1.17(±0.00)	1.02(±0.02)	-	-
MSCIAS (Wang et al., 2019)	80.74(±2.93)	28.36(±1.86)	42.16(±0.47)	5.66(±0.35)	12.98(±0.14)	-	-
MVSC (Gao et al., 2015)	53.68(±9.10)	37.74(±2.22)	-	-	-	-	-
MLRSSC (Brbić & Kopriva, 2018)	63.85(±4.83)	12.11(±0.00)	2.47(±0.00)	2.89(±0.75)	-	-	-
MPAC (Kang et al., 2019)	80.50(±0.00)	45.12(±0.00)	23.56(±0.00)	6.56(±0.00)	-	-	-
MCLES (Chen et al., 2020)	28.12(±1.27)	27.33(±0.74)	16.70(±2.10)	-	-	-	-
FMCNOF (Yang et al., 2021)	51.10(±4.83)	41.78(±3.22)	5.18(±0.02)	3.21(±0.17)	-	11.02(±1.13)	44.82(±2.32)
ADAGAE (Li et al., 2022b)	78.47(±0.37)	39.28(±0.19)	5.23(±0.68)	3.22(±0.27)	-	-	-
PFSC (Lv et al., 2021)	55.85(±2.33)	39.09(±2.55)	-	-	-	-	-
SFMC (Li et al., 2022a)	38.68(±0.00)	45.10(±0.00)	7.95(±0.00)	12.82(±0.00)	12.20(±0.00)	2.90(±0.00)	-
MSGL (Kang et al., 2022)	64.40(±1.21)	-	-	3.66(±0.03)	20.73(±0.76)	10.69(±0.23)	-
FPMVS (Wang et al., 2022d)	81.78(±5.21)	45.00(±1.10)	13.56(±1.67)	5.60(±0.66)	30.23(±3.30)	15.13(±1.16)	58.10(±3.02)
MFLVC (Xu et al., 2022)	81.23(±0.10)	58.74(±0.15)	12.97(±0.14)	3.25(±0.90)	-	-	-
UOMVSC (Tang et al., 2023)	88.24(±0.00)	45.07(±0.00)	21.26(±0.00)	11.17(±0.00)	19.03(±0.00)	-	-
PGSC (Wu et al., 2023)	66.61(±2.84)	33.95(±3.07)	15.92(±1.08)	4.94(±0.80)	22.16(±0.42)	-	-
OrthNTF (Li et al., 2024c)	52.33(±0.00)	42.12(±0.00)	39.74(±0.00)	7.43(±0.00)	28.87(±0.00)	11.58(±0.00)	58.83(±0.00)
FMVACC (Wang et al., 2022c)	80.78(±4.44)	38.41(±2.92)	33.50(±2.56)	9.94(±1.54)	28.50(±2.29)	12.86(±0.67)	57.82(±0.93)
FASTMI (Huang et al., 2023)	81.83(±6.01)	45.05(±1.45)	31.21(±2.89)	7.67(±0.56)	29.29(±1.85)	12.85(±0.32)	59.03(±0.41)
Ours	89.97(±0.00)	45.25(±0.00)	43.70(±0.00)	6.25(±0.00)	31.87(±0.00)	15.64(±0.00)	59.21(±0.00)
			ACC(%)				
FMR (Li et al., 2019)	80.87(±5.92)	39.95(±0.66)	40.54(±1.98)	-	-	-	-
PMSC (Kang et al., 2020a)	80.01(±9.96)	49.92(±2.58)	28.84(±0.74)	23.57(±0.48)	-	-	-
AMGL (Nie et al., 2016)	22.75(±0.31)	39.84(±2.06)	14.99(±0.18)	16.78(±0.01)	17.43(±0.05)	-	-
MSCIAS (Wang et al., 2019)	83.60(±3.85)	43.89(±2.15)	51.64(±2.74)	23.66(±0.42)	34.23(±0.37)	-	-
MVSC (Gao et al., 2015)	55.69(±8.57)	49.86(±2.26)	-	-	-	-	-
MLRSSC (Brbić & Kopriva, 2018)	67.53(±5.04)	57.26(±0.00)	31.08(±0.00)	18.62(±0.34)	-	-	-
MPAC (Kang et al., 2019)	81.84(±0.00)	71.64(±0.00)	40.21(±0.00)	24.79(±0.00)	-	-	-
MCLES (Chen et al., 2020)	46.18(±2.15)	40.47(±1.06)	32.03(±2.33)	-	-	-	-
FMCNOF (Yang et al., 2021)	62.85(±5.32)	71.98(±5.67)	29.10(±2.74)	22.92(±2.57)	-	21.62(±1.83)	41.51(±2.62)
ADAGAE (Li et al., 2022b)	67.88(±0.99)	42.20(±0.94)	23.45(±0.29)	19.43(±1.76)	-	-	-
PFSC (Lv et al., 2021)	52.27(±4.99)	57.87(±5.43)	-	-	-	-	-
SFMC (Li et al., 2022a)	49.44(±0.00)	67.71(±0.00)	30.50(±0.00)	15.86(±0.00)	25.55(±0.00)	9.98(±0.00)	-
MSGL (Kang et al., 2022)	73.46(±0.97)	-	-	20.78(±0.28)	42.65(±0.21)	22.57(±0.43)	-
FPMVS (Wang et al., 2022d)	78.33(±7.05)	61.47(±1.35)	37.12(±2.53)	28.01(±1.20)	51.82(±2.56)	27.12(±0.79)	52.86(±3.35)
MFLVC (Xu et al., 2022)	80.73(±0.47)	43.42(±0.26)	31.02(±0.82)	25.42(±1.47)	-	-	-
UOMVSC (Tang et al., 2023)	77.65(±0.00)	67.10(±0.00)	44.72(±0.00)	23.26(±0.00)	36.28(±0.00)	-	-
PGSC (Wu et al., 2023)	70.08(±6.07)	52.76(±3.07)	29.19(±2.07)	28.13(±1.88)	42.47(±0.89)	-	-
OrthNTF (Li et al., 2024c)	82.43(±0.00)	68.84(±0.00)	47.76(±0.00)	23.36(±0.00)	47.96(±0.00)	25.88(±0.00)	53.27(±0.00)
FMVACC (Wang et al., 2022c)	82.92(±8.57)	39.55(±4.46)	51.70(±3.66)	23.48(±1.98)	54.07(±3.72)	25.69(±0.90)	56.88(±3.09)
FASTMI (Huang et al., 2023)	74.13(±3.36)	53.34(±2.84)	47.10(±4.07)	22.95(±0.89)	42.31(±3.17)	25.58(±0.66)	55.44(±2.25)
Ours	85.47(±0.00)	80.66(±0.00)	52.44(±0.00)	26.22(±0.00)	54.26(±0.00)	26.83(±0.00)	57.36(±0.00)
			Fscore(%)				
FMR (Li et al., 2019)	76.45(±5.48)	45.29(±1.63)	27.83(±1.13)	-	-	-	-
PMSC (Kang et al., 2020a)	80.22(±8.10)	51.13(±2.49)	27.48(±0.67)	26.37(±0.63)	-	-	-
AMGL (Nie et al., 2016)	18.27(±0.12)	40.47(±1.57)	24.78(±0.02)	28.51(±0.00)	28.61(±0.00)	-	-
MSCIAS (Wang et al., 2019)	80.90(±3.07)	42.80(±1.11)	41.84(±1.26)	21.42(±0.36)	33.94(±0.08)	-	-
MVSC (Gao et al., 2015)	54.52(±9.73)	48.53(±1.96)	-	-	-	-	-
MLRSSC (Brbić & Kopriva, 2018)	63.90(±4.48)	49.62(±0.00)	28.87(±0.00)	27.69(±0.41)	-	-	-
MPAC (Kang et al., 2019)	81.01(±0.00)	67.25(±0.00)	29.25(±0.00)	24.29(±0.00)	-	-	-
MCLES (Chen et al., 2020)	39.10(±1.37)	36.16(±0.62)	28.95(±0.82)	-	-	-	-
FMCNOF (Yang et al., 2021)	56.89(±4.24)	67.43(±5.73)	29.89(±4.82)	21.29(±3.14)	-	19.83(±2.77)	36.74(±3.63)
ADAGAE (Li et al., 2022b)	67.74(±0.79)	50.51(±0.41)	23.68(±0.14)	19.61(±1.23)	-	-	-
PFSC (Lv et al., 2021)	55.46(±4.05)	62.75(±7.08)	-	-	-	-	-
SFMC (Li et al., 2022a)	42.90(±0.00)	65.50(±0.00)	30.20(±0.00)	27.69(±0.00)	34.04(±0.00)	18.13(±0.00)	-
MSGL (Kang et al., 2022)	70.39(±0.76)	-	-	24.59(±0.53)	37.57(±0.27)	16.37(±0.86)	-
FPMVS (Wang et al., 2022d)	80.35(±6.83)	62.09(±1.21)	25.36(±1.03)	22.96(±1.16)	42.53(±1.92)	20.31(±0.56)	48.43(±2.66)
MFLVC (Xu et al., 2022)	73.92(±1.63)	52.68(±1.43)	32.41(±1.05)	25.13(±0.67)	-	-	-
UOMVSC (Tang et al., 2023)	79.17(±0.00)	67.85(±0.00)	33.12(±0.00)	28.47(±0.00)	35.23(±0.00)	-	-
PGSC (Wu et al., 2023)	69.15(±5.23)	55.84(±4.70)	29.29(±1.46)	24.88(±0.32)	38.57(±0.85)	-	-
OrthNTF (Li et al., 2024c)	78.43(±0.00)	65.63(±0.00)	37.52(±0.00)	24.77(±0.00)	39.68(±0.00)	16.74(±0.00)	47.67(±0.00)
FMVACC (Wang et al., 2022c)	80.15(±7.13)	41.01(±4.20)	38.20(±1.89)	23.79(±0.77)	43.86(±2.61)	17.07(±0.35)	48.78(±1.94)
FASTMI (Huang et al., 2023)	76.98(±5.19)	56.39(±2.93)	35.19(±2.36)	25.94(±1.21)	39.20(±1.81)	14.35(±0.29)	50.21(±1.25)
Ours	87.92(±0.00)	78.12(±0.00)	41.12(±0.00)	28.55(±0.00)	44.84(±0.00)	20.64(±0.00)	51.37(±0.00)

6.2 Clustering Results and Analysis

We summarize the clustering results in Table 1, and from this table we can conclude that,

1. **Overall Effectiveness.** Our DLA-EF-JA consistently beats these twenty competitors in terms of all three metrics on DERMATO, Reuters, CIF10Tra4 and FasMNI4V. Particularly, it makes 6.91% improvement in Fscore than the second-best approach on DERMATO. In other cases, such as on Cora, it is still able to provide comparable outcomes. These signals that our DLA-EF-JA is effective in partitioning multi-view data and can achieve competitive clustering outcomes.

2. **Anchor Suitability.** In contrast with PMSC, AMGL, MCLES, FMCNOF, OrthNTF, FMR, PGSC, etc, which tackle MVC problems using tensor, kernel, latent space, co-training or matrix factorization means, our DLA-EF-JA using anchor tool can produce better results than them. For instance, on Cora, it surpasses them in terms of NMI with 38.59%, 42.37%, 27.00%, 42.63%, 43.20%, 23.07%, 42.55%, respectively. These suggest that our adopted anchor means is recommendable.

3. **Ample Affinity.** Different from FPMVS, FMVACC, FASTMI, SFMC, etc, which concentrate only on the anchor-sample relationship, DLA-EF-JA also successfully takes anchor-anchor characteristics into the measuring of overall similarity and accordingly brings performance enhancement. Taking FASTMI as an example, DLA-EF-JA outperforms it on all of these seven datasets and three metrics, which reveals that our dual-level affinity strategy can help extract representations more fully.

4. **Reliable Stability.** The results outputted by our DLA-EF-JA are all not with variance. This mainly benefits from avoiding the generation of embedding. Not only does the embedding-free property enhance the stability, but allows the labels to be directly derived from original data, well maintaining the diversity. Despite non-variance for MPAC, SFMC and Orth, the low-rank constraint could damage potential graph structure, accordingly weakening their performance.

5. **Flexible Alignment.** Compared to FMVACC that requires firstly selecting the baseline view and then performs alignment based on completed anchors, DLA-EF-JA exceeds it with remarkable margins. For example on CALTE7, DLA-EF-JA receives 6.84%, 41.11%, 37.11% improvement respectively. This is primarily because our joint-alignment strategy, besides not involving the baseline view, can also coordinate with the generation of anchors, more flexibly transforming anchors to align.

6. **Broader Applicability.** Some methods like PMSC, PFSC, MFLVC, AMGL, UOMVSC, MCLES, PGSC, etc, can not work with large-sized CIF10Tra4 and FasMNI4V due to the intensive complexities or self-limitations, while our proposed DLA-EF-JA operates normally with its lower complexities and meanwhile can produce superior clustering outcomes. So, DLA-EF-JA enjoys broader applicability.

Due to the space limit, more conclusions are presented in the Section F of Appendix.

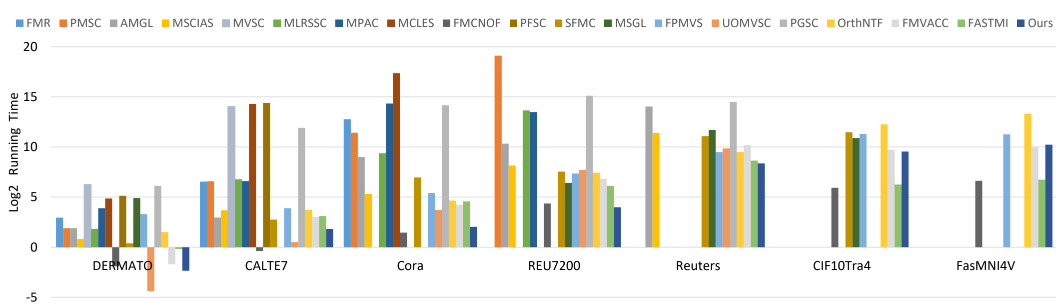

Figure 2: The running time comparison between algorithms on seven public benchmark datasets.

6.3 Running Time Comparison

To illustrate the efficiency of DLA-EF-JA, we count the running time of each algorithm, and report the comparison results in Fig. (2). From this figure, we can draw that,

1. MVSC, PFSC, PGSC and MCLES consume significantly more time than others. This is mainly caused by the subspace strategy they employed, which typically requires constructing large-sized similarity and needs at least cubic computational overhead.

2. MPAC, PMSC, FMR, MLRSSC, etc, take more time than us, which is mainly because MPAC and PMSC gather multi-view representations at the partition level, and FMR and MLRSSC utilize the kernel dependence measure to do data reconstruction.

3. FPMVS, FMVACC, MSGL and SFMC operates slower than us. Possible reasons are that the connection component constraints and feature matching constraints conducted on anchor graph induce a large proportion of additional time expenditure.

4. FMCNOF and FASTMI enjoy slightly faster running speed, the reasons of which could be that FMCNOF decouples dense optimization matrices by sparse factorization skills and FASTMI generates base clusterings via fast partitioning on the view-sharing graph.

5. AMGL, MSCIAS, UOMVSC and OrthNTF are generally faster than PMSC, MVSC, PGSC, MPAC, PFSC, etc, possibly because the former ones alleviate the computing burden of spectral partitioning and graph mergence via low-rank approximation or non-negative factorization.

6. All algorithms can normally work on DERMATO and CALTE7, while with the increase of sample size, PFSC, FMR, MCLES, PMSC, MPAC, MSGL, etc, are gradually ineffective, which is mainly due to the limitations of their innate computing requirement or memory cost.

6.4 Ablation Study

To validate the effectiveness of dual-level affinity (DLA), we organize relevant ablation experiments and present the comparison results in Table 2 where SLA denotes the clustering results of considering only anchor-sample relation. As seen, our DLA is coherently better than SLA, which well illustrates that DLA can help achieve superior results.

Table 2: The effectiveness of dual-level affinity

Metric	Ablation	DERMATO	CALTE7	Cora	REU7200	Reuters	CIF10Tra4	FasMNI4V
NMI	SLA	83.97	40.21	6.02	2.53	23.19	15.48	58.13
	DLA	**89.97**	**45.25**	**43.70**	**6.25**	**31.87**	**15.64**	**59.21**
ACC	SLA	71.51	49.05	30.35	16.75	47.05	26.69	52.15
	DLA	**85.47**	**80.66**	**52.44**	**26.22**	**54.26**	**26.83**	**57.36**
Fscore	SLA	73.79	51.25	30.42	28.54	43.04	17.70	46.77
	DLA	**87.92**	**78.12**	**41.12**	**28.55**	**44.84**	**20.64**	**51.37**

Table 3 summarizes the ablation results about our embedding-free (EF) strategy, where CE denotes the clustering results containing embedding. Evidently, in addition to owning the ability to generate preferable and stable clustering results, our EF also enjoys less time consuming. This indicates that our EF is more suitable for MVC problems.

Table 3: The effectiveness of embedding-free strategy

Metric	Ablation	DERMATO	CALTE7	Cora	REU7200	Reuters	CIF10Tra4	FasMNI4V
NMI	CE	84.32(±1.32)	40.63(±1.89)	40.02(±2.31)	6.02(±0.68)	26.23(±1.37)	12.22(±0.97)	**60.14(±0.36)**
	EF	**89.97(±0.00)**	**45.25(±0.00)**	**43.70(±0.00)**	**6.25(±0.00)**	**31.87(±0.00)**	**15.64(±0.00)**	59.21(±0.00)
ACC	CE	81.33(±1.82)	74.74(±1.73)	48.27(±1.07)	23.46(±0.79)	**55.78(±1.62)**	22.64(±1.07)	55.03(±0.92)
	EF	**85.47(±0.00)**	**80.66(±0.00)**	**52.44(±0.00)**	**26.22(±0.00)**	54.26(±0.00)	**26.83(±0.00)**	**57.36(±0.00)**
Fscore	CE	79.67(±2.07)	71.37(±1.13)	35.92(±1.96)	22.82(±1.02)	41.03(±0.93)	19.26(±1.63)	46.86(±0.87)
	EF	**87.92(±0.00)**	**78.12(±0.00)**	**41.12(±0.00)**	**28.55(±0.00)**	**44.84(±0.00)**	**20.64(±0.00)**	**51.37(±0.00)**
Time(s)	CE	0.83	9.81	11.53	51.24	892.17	2003.72	3850.35
	EF	**0.20**	**3.53**	**4.07**	**15.73**	**330.21**	**746.76**	**1193.83**

In the paper we adopt a joint-alignment (JA) strategy to decrease the mismatching risk. To demonstrate its effectiveness, we report the ablation results in Table 4, where UA denotes the clustering results without involving alignment. It is easy to discover that JA makes more favorable results than UA, which suggests that our JA is functional.

Table 4: The effectiveness of joint-alignment

Metric	Ablation	DERMATO	CALTE7	Cora	REU7200	Reuters	CIF10Tra4	FasMNI4V
NMI	UA	82.53	39.55	35.41	3.32	24.77	15.30	56.47
	JA	**89.97**	**45.25**	**43.70**	**6.25**	**31.87**	**15.64**	**59.21**
ACC	UA	80.73	76.59	31.65	16.67	45.29	25.91	53.68
	JA	**85.47**	**80.66**	**52.44**	**26.22**	**54.26**	**26.83**	**57.36**
Fscore	UA	79.47	72.23	30.69	21.14	42.59	17.90	47.41
	JA	**87.92**	**78.12**	**41.12**	**28.55**	**44.84**	**20.64**	**51.37**

7 Limitations

DLA-EF-JA contains hyper-parameters λ and β, which requires additional efforts for fine-tuning. Thus, designing a non-parametric version can further boost its practicality. Besides, we adopt the square weighting scheme with linear constraints to measure the contributions between views. Some other view schemes could be deeply investigated in the future so as to further increase the results.

8 Conclusion

In this work, we introduce dual-level affinity, which concurrently considers anchor-sample and anchor-anchor characteristics, to more fully extract multi-view representations for better clustering. To reduce the mismatching risk, we adopt a joint-alignment mechanism that does not involve the selection of baseline view and also can coordinate with the anchor generation. Furthermore, we avoid forming embedding and directly generate cluster indicators via a binary learning strategy, which not only effectively eliminates the variance but well preserves original diversity. For the resulting optimization problem, we provide a solution with linear complexities. Experiments on multiple public benchmark datasets verify the effectiveness of our proposed DLA-EF-JA. In future work, we will extend our DLA-EF-JA method to non-parametric scenarios to further enhance its practicality.

REFERENCES

Maria Brbić and Ivica Kopriva. Multi-view low-rank sparse subspace clustering. *Pattern Recognition*, 73:247–258, 2018.

Jie Chen, Hua Mao, Dezhong Peng, Changqing Zhang, and Xi Peng. Multiview clustering by consensus spectral rotation fusion. *IEEE Transactions on Image Processing*, 2023a.

Man-Sheng Chen, Ling Huang, Chang-Dong Wang, and Dong Huang. Multi-view clustering in latent embedding space. In *Proceedings of the AAAI Conference on Artificial Intelligence*, volume 34, pp. 3513–3520, 2020.

Man-Sheng Chen, Chang-Dong Wang, Dong Huang, Jian-Huang Lai, and Philip S Yu. Efficient orthogonal multi-view subspace clustering. In *Proceedings of the 28th ACM SIGKDD Conference on Knowledge Discovery and Data Mining*, pp. 127–135, 2022.

Man-Sheng Chen, Chang-Dong Wang, and Jian-Huang Lai. Low-rank tensor based proximity learning for multi-view clustering. *IEEE Transactions on Knowledge and Data Engineering*, 35 (5):5076–5090, 2023b.

Man-Sheng Chen, Chang-Dong Wang, Dong Huang, Jian-Huang Lai, and S Yu Philip. Concept factorization based multiview clustering for large-scale data. *IEEE Transactions on Knowledge and Data Engineering*, 2024.

Yongyong Chen, Xiaojia Zhao, Zheng Zhang, Youfa Liu, Jingyong Su, and Yicong Zhou. Tensor learning meets dynamic anchor learning: From complete to incomplete multiview clustering. *IEEE Transactions on Neural Networks and Learning Systems*, 2023c.

Chenhang Cui, Yazhou Ren, Jingyu Pu, Jiawei Li, Xiaorong Pu, Tianyi Wu, Yutao Shi, and Lifang He. A novel approach for effective multi-view clustering with information-theoretic perspective. *Advances in Neural Information Processing Systems*, 36, 2024.

Si-Guo Fang, Dong Huang, Xiao-Sha Cai, Chang-Dong Wang, Chaobo He, and Yong Tang. Efficient multi-view clustering via unified and discrete bipartite graph learning. *IEEE Transactions on Neural Networks and Learning Systems*, 2023.

Yulu Fu, Yuting Li, Qiong Huang, Jinrong Cui, and Jie Wen. Anchor graph network for incomplete multiview clustering. *IEEE Transactions on Neural Networks and Learning Systems*, 2024.

Hongchang Gao, Feiping Nie, Xuelong Li, and Heng Huang. Multi-view subspace clustering. In *Proceedings of the IEEE International Conference on Computer Vision*, pp. 4238–4246, 2015.

Wenjue He, Zheng Zhang, Yongyong Chen, and Jie Wen. Structured anchor-inferred graph learning for universal incomplete multi-view clustering. *World Wide Web*, 26(1):375–399, 2023.

Dong Huang, Chang-Dong Wang, Jian-Huang Lai, and Chee-Keong Kwoh. Toward multidiversified ensemble clustering of high-dimensional data: From subspaces to metrics and beyond. *IEEE Transactions on Cybernetics*, 52(11):12231–12244, 2022.

Dong Huang, Chang-Dong Wang, and Jian-Huang Lai. Fast multi-view clustering via ensembles: Towards scalability, superiority, and simplicity. *IEEE Transactions on Knowledge and Data Engineering*, 35(11):11388–11402, 2023.

Dong Huang, Ding-Hua Chen, Xiangji Chen, Chang-Dong Wang, and Jian-Huang Lai. Deepclue: Enhanced deep clustering via multi-layer ensembles in neural networks. *IEEE Transactions on Emerging Topics in Computational Intelligence*, 2024a.

Dong Huang, Xiaozhi Deng, Ding-Hua Chen, Zihao Wen, Weijun Sun, Chang-Dong Wang, and Jian-Huang Lai. Deep clustering with hybrid-grained contrastive and discriminative learning. *IEEE Transactions on Circuits and Systems for Video Technology*, 2024b.

Zhao Kang, Zipeng Guo, Shudong Huang, Siying Wang, Wenyu Chen, Yuanzhang Su, and Zenglin Xu. Multiple partitions aligned clustering. In *Proceedings of the 28th International Joint Conference on Artificial Intelligence*, pp. 2701–2707, 2019.

Zhao Kang, Xinjia Zhao, Chong Peng, Hongyuan Zhu, Joey Tianyi Zhou, Xi Peng, Wenyu Chen, and Zenglin Xu. Partition level multiview subspace clustering. *Neural Networks*, 122:279–288, 2020a.

Zhao Kang, Wangtao Zhou, Zhitong Zhao, Junming Shao, Meng Han, and Zenglin Xu. Large-scale multi-view subspace clustering in linear time. In *Proceedings of the AAAI conference on artificial intelligence*, volume 34, pp. 4412–4419, 2020b.

Zhao Kang, Zhiping Lin, Xiaofeng Zhu, and Wenbo Xu. Structured graph learning for scalable subspace clustering: From single view to multiview. *IEEE Transactions on Cybernetics*, 52(9): 8976–8986, 2022.

Jinghuan Lao, Dong Huang, Chang-Dong Wang, and Jian-Huang Lai. Towards scalable multi-view clustering via joint learning of many bipartite graphs. *IEEE Transactions on Big Data*, 10(01): 77–91, 2024.

Jing Li, Qianqian Wang, Ming Yang, Quanxue Gao, and Xinbo Gao. Efficient anchor graph factorization for multi-view clustering. *IEEE Transactions on Multimedia*, 2023.

Jing Li, Quanxue Gao, Qianqian Wang, Cheng Deng, and Deyan Xie. Label learning method based on tensor projection. In *Proceedings of the 30th ACM SIGKDD Conference on Knowledge Discovery and Data Mining*, pp. 1599–1609, 2024a.

Jing Li, Quanxue Gao, Qianqian Wang, and Wei Xia. Tensorized label learning on anchor graph. In *Proceedings of the AAAI Conference on Artificial Intelligence*, volume 38, pp. 13537–13544, 2024b.

Jing Li, Quanxue Gao, Qianqian Wang, Ming Yang, and Wei Xia. Orthogonal non-negative tensor factorization based multi-view clustering. *Advances in Neural Information Processing Systems*, 36, 2024c.

Ruihuang Li, Changqing Zhang, Qinghua Hu, Pengfei Zhu, and Zheng Wang. Flexible multi-view representation learning for subspace clustering. In *Proceedings of the 28th International Joint Conference on Artificial Intelligence*, pp. 2916–2922, 2019.

Xingfeng Li, Yuangang Pan Pan, Yinghui Sun, Quansen Sun Sun, Ivor W Tsang, and Zhenwen Ren. Fast unpaired multi-view clustering. In *Proceedings of the 33rd International Joint Conference on Artificial Intelligence*, 2024d.

Xuelong Li, Han Zhang, Rong Wang, and Feiping Nie. Multiview clustering: A scalable and parameter-free bipartite graph fusion method. *IEEE Transactions on Pattern Analysis and Machine Intelligence*, 44(1):330–344, 2022a.

Xuelong Li, Hongyuan Zhang, and Rui Zhang. Adaptive graph auto-encoder for general data clustering. *IEEE Transactions on Pattern Analysis and Machine Intelligence*, 44(12):9725–9732, 2022b.

Suyuan Liu, Ke Liang, Zhibin Dong, Siwei Wang, Xihong Yang, Sihang Zhou, En Zhu, and Xinwang Liu. Learn from view correlation: An anchor enhancement strategy for multi-view clustering. In *Proceedings of the IEEE/CVF Conference on Computer Vision and Pattern Recognition*, pp. 26151–26161, 2024.

Zhen Long, Qiyuan Wang, Yazhou Ren, Yipeng Liu, and Ce Zhu. S2mvtc: a simple yet efficient scalable multi-view tensor clustering. In *Proceedings of the IEEE/CVF Conference on Computer Vision and Pattern Recognition*, pp. 26213–26222, 2024.

Yiding Lu, Yijie Lin, Mouxing Yang, Dezhong Peng, Peng Hu, and Xi Peng. Decoupled contrastive multi-view clustering with high-order random walks. In *Proceedings of the AAAI Conference on Artificial Intelligence*, volume 38, pp. 14193–14201, 2024.

Juncheng Lv, Zhao Kang, Boyu Wang, Luping Ji, and Zenglin Xu. Multi-view subspace clustering via partition fusion. *Information Sciences*, 560:410–423, 2021.

Feiping Nie, Jing Li, and Xuelong Li. Parameter-free auto-weighted multiple graph learning: a framework for multiview clustering and semi-supervised classification. In *Proceedings of the Twenty-Fifth International Joint Conference on Artificial Intelligence*, pp. 1881–1887, 2016.

Feiping Nie, Fangyuan Xie, Weizhong Yu, and Xuelong Li. Parameter-insensitive min cut clustering with flexible size constrains. *IEEE Transactions on Pattern Analysis and Machine Intelligence*, 2024a.

Feiping Nie, Jingjing Xue, Weizhong Yu, and Xuelong Li. Fast clustering with anchor guidance. *IEEE Transactions on Pattern Analysis and Machine Intelligence*, 46(4):1898–1912, 2024b.

Qianyao Qiang, Bin Zhang, Fei Wang, and Feiping Nie. Fast multi-view discrete clustering with anchor graphs. In *Proceedings of the AAAI Conference on Artificial Intelligence*, volume 35, pp. 9360–9367, 2021.

Yalan Qin, Hanzhou Wu, Xinpeng Zhang, and Guorui Feng. Semi-supervised structured subspace learning for multi-view clustering. *IEEE Transactions on Image Processing*, 31:1–14, 2022.

Shaojun Shi, Feiping Nie, Rong Wang, and Xuelong Li. Fast multi-view clustering via prototype graph. *IEEE Transactions on Knowledge and Data Engineering*, 35(1):443–455, 2021.

Chang Tang, Zhenglai Li, Jun Wang, Xinwang Liu, Wei Zhang, and En Zhu. Unified one-step multi-view spectral clustering. *IEEE Transactions on Knowledge and Data Engineering*, 35(06): 6449–6460, 2023.

Huayi Tang and Yong Liu. Deep safe multi-view clustering: Reducing the risk of clustering performance degradation caused by view increase. In *Proceedings of the IEEE/CVF Conference on Computer Vision and Pattern Recognition*, pp. 202–211, 2022.

Jingyu Wang, Zhenyu Ma, Feiping Nie, and Xuelong Li. Fast self-supervised clustering with anchor graph. *IEEE Transactions on Neural Networks and Learning Systems*, 33(9):4199–4212, 2022a.

Jun Wang, Chang Tang, Zhiguo Wan, Wei Zhang, Kun Sun, and Albert Y Zomaya. Efficient and effective one-step multiview clustering. *IEEE Transactions on Neural Networks and Learning Systems*, 2023a.

Qianqian Wang, Jiafeng Cheng, Quanxue Gao, Guoshuai Zhao, and Licheng Jiao. Deep multi-view subspace clustering with unified and discriminative learning. *IEEE Transactions on Multimedia*, 23:3483–3493, 2021.

Qianqian Wang, Zhengming Ding, Zhiqiang Tao, Quanxue Gao, and Yun Fu. Generative partial multi-view clustering with adaptive fusion and cycle consistency. *IEEE Transactions on Image Processing*, 30:1771–1783, 2022b.

Qianqian Wang, Zhiqiang Tao, Wei Xia, Quanxue Gao, Xiaochun Cao, and Licheng Jiao. Adversarial multiview clustering networks with adaptive fusion. *IEEE Transactions on Neural Networks and Learning Systems*, 34(10):7635–7647, 2023b.

Qianqian Wang, Zhiqiang Tao, Quanxue Gao, and Licheng Jiao. Multi-view subspace clustering via structured multi-pathway network. *IEEE Transactions on Neural Networks and Learning Systems*, 35(5):7244–7250, 2024.

Siwei Wang, Xinwang Liu, Suyuan Liu, Jiaqi Jin, Wenxuan Tu, Xinzhong Zhu, and En Zhu. Align then fusion: Generalized large-scale multi-view clustering with anchor matching correspondences. *Advances in Neural Information Processing Systems*, 35:5882–5895, 2022c.

Siwei Wang, Xinwang Liu, Xinzhong Zhu, Pei Zhang, Yi Zhang, Feng Gao, and En Zhu. Fast parameter-free multi-view subspace clustering with consensus anchor guidance. *IEEE Transactions on Image Processing*, 31:556–568, 2022d.

Xiaobo Wang, Zhen Lei, Xiaojie Guo, Changqing Zhang, Hailin Shi, and Stan Z Li. Multi-view subspace clustering with intactness-aware similarity. *Pattern Recognition*, 88:50–63, 2019.

Jie Wen, Chengliang Liu, Gehui Xu, Zhihao Wu, Chao Huang, Lunke Fei, and Yong Xu. Highly confident local structure based consensus graph learning for incomplete multi-view clustering. In *Proceedings of the IEEE/CVF Conference on Computer Vision and Pattern Recognition*, pp. 15712–15721, 2023a.

Jie Wen, Zheng Zhang, Lunke Fei, Bob Zhang, Yong Xu, Zhao Zhang, and Jinxing Li. A survey on incomplete multiview clustering. *IEEE Transactions on Systems, Man, and Cybernetics: Systems*, 53(2):1136–1149, 2023b.

Jie Wen, Shijie Deng, Waikeung Wong, Guoqing Chao, Chao Huang, Lunke Fei, and Yong Xu. Diffusion-based missing-view generation with the application on incomplete multi-view clustering. In *Forty-first International Conference on Machine Learning*. PMLR, 2024a.

Jie Wen, Gehui Xu, Zhanyan Tang, Wei Wang, Lunke Fei, and Yong Xu. Graph regularized and feature aware matrix factorization for robust incomplete multi-view clustering. *IEEE Transactions on Circuits and Systems for Video Technology*, 34(5):3728–3741, 2024b.

Hongjie Wu, Shudong Huang, Chenwei Tang, Yancheng Zhang, and Jiancheng Lv. Pure graph-guided multi-view subspace clustering. *Pattern Recognition*, 136:109187, 2023.

Wei Xia, Quanxue Gao, Qianqian Wang, and Xinbo Gao. Tensor completion-based incomplete multiview clustering. *IEEE Transactions on Cybernetics*, 52(12):13635–13644, 2022a.

Wei Xia, Quanxue Gao, Qianqian Wang, Xinbo Gao, Chris Ding, and Dacheng Tao. Tensorized bipartite graph learning for multi-view clustering. *IEEE Transactions on Pattern Analysis and Machine Intelligence*, 2022b.

Wei Xia, Qianqian Wang, Quanxue Gao, Xiangdong Zhang, and Xinbo Gao. Self-supervised graph convolutional network for multi-view clustering. *IEEE Transactions on Multimedia*, 24:3182–3192, 2022c.

Wei Xia, Xiangdong Zhang, Quanxue Gao, Xiaochuang Shu, Jungong Han, and Xinbo Gao. Multi-view subspace clustering by an enhanced tensor nuclear norm. *IEEE Transactions on Cybernetics*, 52(9):8962–8975, 2022d.

Jie Xu, Yazhou Ren, Guofeng Li, Lili Pan, Ce Zhu, and Zenglin Xu. Deep embedded multi-view clustering with collaborative training. *Information Sciences*, 573:279–290, 2021a.

Jie Xu, Yazhou Ren, Huayi Tang, Xiaorong Pu, Xiaofeng Zhu, Ming Zeng, and Lifang He. Multi-vae: Learning disentangled view-common and view-peculiar visual representations for multi-view clustering. In *Proceedings of the IEEE/CVF International Conference on Computer Vision*, pp. 9234–9243, 2021b.

Jie Xu, Huayi Tang, Yazhou Ren, Liang Peng, Xiaofeng Zhu, and Lifang He. Multi-level feature learning for contrastive multi-view clustering. In *Proceedings of the IEEE/CVF Conference on Computer Vision and Pattern Recognition*, pp. 16051–16060, 2022.

Jie Xu, Chao Li, Liang Peng, Yazhou Ren, Xiaoshuang Shi, Heng Tao Shen, and Xiaofeng Zhu. Adaptive feature projection with distribution alignment for deep incomplete multi-view clustering. *IEEE Transactions on Image Processing*, 32:1354–1366, 2023a.

Jie Xu, Yazhou Ren, Huayi Tang, Zhimeng Yang, Lili Pan, Yang Yang, Xiaorong Pu, Philip S Yu, and Lifang He. Self-supervised discriminative feature learning for deep multi-view clustering. *IEEE Transactions on Knowledge and Data Engineering*, 35(7):7470–7482, 2023b.

Jie Xu, Yazhou Ren, Xiaolong Wang, Lei Feng, Zheng Zhang, Gang Niu, and Xiaofeng Zhu. Investigating and mitigating the side effects of noisy views for self-supervised clustering algorithms in practical multi-view scenarios. In *Proceedings of the IEEE/CVF Conference on Computer Vision and Pattern Recognition*, pp. 22957–22966, 2024.

Weiqing Yan, Jindong Xu, Jinglei Liu, Guanghui Yue, and Chang Tang. Bipartite graph-based discriminative feature learning for multi-view clustering. In *Proceedings of the 30th ACM International Conference on Multimedia*, pp. 3403–3411, 2022.

Ben Yang, Xuetao Zhang, Feiping Nie, Fei Wang, Weizhong Yu, and Rong Wang. Fast multi-view clustering via nonnegative and orthogonal factorization. *IEEE Transactions on Image Processing*, 30:2575–2586, 2021.

Haizhou Yang, Quanxue Gao, Wei Xia, Ming Yang, and Xinbo Gao. Multiview spectral clustering with bipartite graph. *IEEE Transactions on Image Processing*, 31:3591–3605, 2022.

Weizhong Yu, Liyin Xing, Feiping Nie, and Xuelong Li. Multi-view fuzzy clustering based on anchor graph. *IEEE Transactions on Fuzzy Systems*, 2023.

Pengxin Zeng, Mouxing Yang, Yiding Lu, Changqing Zhang, Peng Hu, and Xi Peng. Semantic invariant multi-view clustering with fully incomplete information. *IEEE Transactions on Pattern Analysis and Machine Intelligence*, 46(4):2139–2150, 2023.

Pengxin Zeng, Mouxing Yang, Yiding Lu, Changqing Zhang, Peng Hu, and Xi Peng. Semantic invariant multi-view clustering with fully incomplete information. *IEEE Transactions on Pattern Analysis and Machine Intelligence*, 46(4):2139–2150, 2024.

Changqing Zhang, Huazhu Fu, Qinghua Hu, Xiaochun Cao, Yuan Xie, Dacheng Tao, and Dong Xu. Generalized latent multi-view subspace clustering. *IEEE Transactions on Pattern Analysis and Machine Intelligence*, 42(1):86–99, 2020a.

Changqing Zhang, Huazhu Fu, Jing Wang, Wen Li, Xiaochun Cao, and Qinghua Hu. Tensorized multi-view subspace representation learning. *International Journal of Computer Vision*, 128(8): 2344–2361, 2020b.

Changqing Zhang, Yajie Cui, Zongbo Han, Joey Tianyi Zhou, Huazhu Fu, and Qinghua Hu. Deep partial multi-view learning. *IEEE Transactions on Pattern Analysis and Machine Intelligence*, 44 (05):2402–2415, 2022.

Han Zhang, Feiping Nie, and Xuelong Li. Large-scale clustering with structured optimal bipartite graph. *IEEE Transactions on Pattern Analysis and Machine Intelligence*, 45(8):9950–9963, 2023.

Zheng Zhang, Li Liu, Fumin Shen, Heng Tao Shen, and Ling Shao. Binary multi-view clustering. *IEEE Transactions on Pattern Analysis and Machine Intelligence*, 41(7):1774–1782, 2019.

Wenhui Zhao, Qin Li, Huafu Xu, Quanxue Gao, Qianqian Wang, and Xinbo Gao. Anchor graph-based feature selection for one-step multi-view clustering. *IEEE Transactions on Multimedia*, 2024.

APPENDIX

A NOTATIONS

For more clarity, we summary the utilized symbols and their corresponding meaning, as shown in Table 5.

Table 5: The description of symbols used in this article

Symbol	Meaning
n	the number of samples
m	the number of anchors
v	the number of views
k	the number of clusters
d_p	the data dimension on view p
$\mathbf{X}_p \in \mathbb{R}^{d_p \times n}$	the data matrix on view p
$\mathbf{A}_p \in \mathbb{R}^{d_p \times m}$	the anchor matrix on view p
$\mathbf{T}_p \in \mathbb{R}^{m \times m}$	the permutation matrix on view p
$\mathbf{B}_p \in \mathbb{R}^{m \times k}$	the basic coefficient matrix on view p
$\mathbf{C} \in \mathbb{R}^{k \times n}$	the cluster indicator matrix
$\mathbf{S}_p \in \mathbb{R}^{m \times m}$	the anchor self-expression matrix on view p
$\mathbf{D}_p \in \mathbb{R}^{m \times m}$	the degree matrix of $\mathbf{S}_p$ on view p
$\boldsymbol{\alpha} \in \mathbb{R}^{v \times 1}$	the view weighting vector
$\mathbf{Z}_p \in \mathbb{R}^{m \times n}$	the anchor graph on view p
$\mathbf{L}_\mathbf{s} \in \mathbb{R}^{m \times m}$	the Laplacian matrix about $\mathbf{S}_p$
$\mathbf{E}_p \in \mathbb{R}^{m \times n}$	$\mathbf{T}_p\mathbf{B}_p\mathbf{C}$
$\mathbf{F}_p \in \mathbb{R}^{m \times m}$	$\mathbf{T}_p - \mathbf{T}_p\mathbf{S}_p$
$\mathbf{G}_p \in \mathbb{R}^{m \times m}$	$\mathbf{A}_p^\top \mathbf{A}_p$
$\mathbf{H}_p \in \mathbb{R}^{m \times m}$	$\mathbf{S}_p\mathbf{S}_p^\top$
$\mathbf{M}_p \in \mathbb{R}^{m \times m}$	$\mathbf{B}_p\mathbf{C}\mathbf{C}^\top\mathbf{B}_p^\top$
$\mathbf{J}_p \in \mathbb{R}^{m \times m}$	$\mathbf{A}_p^\top\mathbf{X}_p\mathbf{C}^\top\mathbf{B}_p^\top$
$\mathbf{Q}_p \in \mathbb{R}^{m \times m}$	$\mathbf{T}_p^\top\mathbf{A}_p^\top\mathbf{A}_p\mathbf{T}_p$
$\mathbf{Z} \in \mathbb{R}^{n \times k}$	$2\sum_{p=1}^{v} \boldsymbol{\alpha}_p^2 \mathbf{X}_p^\top \mathbf{A}_p \mathbf{T}_p \mathbf{B}_p$
$\mathbf{W} \in \mathbb{R}^{k \times k}$	$\sum_{p=1}^{v} \boldsymbol{\alpha}_p^2 \mathbf{B}_p^\top \mathbf{T}_p^\top \mathbf{A}_p^\top \mathbf{A}_p \mathbf{T}_p \mathbf{B}_p + \beta \mathbf{B}_p^\top \mathbf{L}_\mathbf{s} \mathbf{B}_p$

B BRIEF INTRODUCTION OF 20 COMPARISON ALGORITHMS

To demonstrate the strong points of the proposed DLA-EF-JA, we select 20 remarkable MVC algorithms as baselines. Their brief introduction is as follows,

1. **FMR (Li et al., 2019):** This method utilizes kernel dependence measure instead of projecting original samples to enhance the correlation between different views, and highlights the comprehensiveness of potential representations through subspace reconstruction.
2. **PMSC (Kang et al., 2020a):** This method merges view information in the level of partition spaces via ensemble learning, and integrates consensus clustering and graph generation to maintain the consistence among views.
3. **AMGL (Nie et al., 2016):** This method assigns a group of weights for all graphs to increase the diversity automatically, and reformulates conventional spectral partitioning procedure into a convex problem so as to generate the optimal solution.

4. **MSCIAS (Wang et al., 2019):** This method maximizes the dependence between intact points by constructing an informative affinity matrix, and avoids view information imbalance by guiding intactness-aware relationship construction using HSIC criterion.
5. **MVSC (Gao et al., 2015):** This method conducts subspace clustering on each view concurrently to explore specific characteristics, and employs an indicator matrix that is shared for all the views to preserve the cluster consistence.
6. **MLRSSC (Brbić & Kopriva, 2018):** This method generates a common similarity matrix with low-rank and sparsity properties to learn joint subspace representations, and utilizes the kernel extension skill to optimize the objective in Hilbert space.
7. **MPAC (Kang et al., 2019):** This method aligns each partition alternatively using a permutation matrix to formulate agreement cluster indicator, and performs graph learning and data partitioning jointly in one common framework to facilitate each other.
8. **MCLES (Chen et al., 2020):** This method tries to capture global structure by exploring embedding representations in latent space, and concurrently learns the cluster labels and similarity matrix without requiring subsequent spectral grouping procedure.
9. **FMCNOF (Yang et al., 2021):** This method integrates matrix factorization and bipartite graph construction together to improve the computational cost, and embeds the factor matrix into cluster matrix to avoid extra k-means operation.
10. **ADAGAE (Li et al., 2022b):** This method extends graph neural network into data clustering task, and takes advantages of auto-encoder and weighted graphs to exploit non-euclidean geometric characteristics and high-level representations.
11. **PFSC (Lv et al., 2021):** This method finds a common partition by collaboratively learning multiple basic partitions to improve the robustness to noise, and jointly performs basic partition generation and unified graph learning to achieve mutual co-evolution.
12. **SFMC (Li et al., 2022a):** This method coalesces view-specific costs to seek for a joint graph that is compatible among views, and indicates clusters straightforwardly by employing connectivity constraint on the joint graph.
13. **MSGL (Kang et al., 2022):** This method discriminates landmarks by building a dictionary matrix to decrease the cost of graph generation, and discovers a graph with explicit components to preserve the data manifold.
14. **FPMVS (Wang et al., 2022d):** This method designs a group of space-guided projection matrices to alleviate the dimension inconsistency in common space, and determines the contribution of each individual view to the unified graph in a learnable manner.
15. **MFLVC (Xu et al., 2022):** This method jointly realizes view-specific reconstruction objective and semantic consistency objectives by learning diverse levels of representations in a fusion-free way, and utilizes the common semantics to generate the clustering labels.
16. **UOMVSC (Tang et al., 2023):** This method unifies the spectral embedding and spectral discretization via one-pass strategy to alleviate the information loss caused by the two-step process, and approximates the rank of affinity graph through the inner product of embedding matrices.
17. **PGSC (Wu et al., 2023):** This method exploits the connectivity and sparsity of each similarity graph to achieve the pure graph with a block-diagonal structure, and assigns labels directly by enforcing it including corresponding connection components.
18. **OrthNTF (Li et al., 2024c):** This method establishes an orthogonal non-negative tensor factorization scheme to directly consider the cross-correlation between views, and extracts complementary information hidden in multi-view samples through tensor regularization.
19. **FMVACC (Wang et al., 2022c):** This method associates each view with one permutation matrix to flexibly rearrange all similarity graphs column-wisely, and enhances the accuracy of graph fusion by utilizing both feature and structure information.
20. **FASTMI (Huang et al., 2023):** This method achieves multi-stage mergence by building view-wise relations using random view grouping, and utilizes a graph partitioning mechanism to generate basic clusterings for each view group.

C BRIEF INTRODUCTION OF 7 PUBLIC BENCHMARK DATASETS

In experiments, we evaluate the algorithm performance on 7 public benchmark datasets, and their brief introduction is as follows,

1. **DERMATO:** This is a skin image dataset and consists of 358 samples. It contains 2 views and 6 clusters. The feature dimensions on each view are 12 and 22 respectively.
2. **CALTE7:** This is an object image dataset and consists of 1474 samples. It contains 6 views and 7 clusters. The feature dimensions on each view are 48, 40, 254, 1984, 512 and 928, respectively.
3. **Cora:** This citation network dataset has 2708 samples, and includes 4 views and 7 clusters. The feature dimensions on each view are 2708, 1433, 2708 and 2708, respectively.
4. **REU7200:** This document dataset has 7200 samples, and includes 5 views and 6 clusters. The feature dimensions on each view are 4819, 4810, 4892, 4858 and 4777, respectively.
5. **Reuters:** This is a news article dataset with 18758 samples, and involves 5 views and 6 clusters. The feature dimensions on each view are 21531, 24892, 34251, 15506 and 11547, respectively.
6. **CIF10Tra4:** This is a color image dataset with 50000 samples, and involves 4 views and 10 clusters. The feature dimensions on each view are 944, 576, 512 and 640, respectively.
7. **FasMNI4V:** This is a fashion product image dataset with 70000 samples, and involves 4 views and 10 clusters. The feature dimensions on each view are 512, 576, 640 and 944, respectively.

D MORE RELATED WORK

To effectively tackle MVC tasks, Chen et al. (2022) utilize the algebraic property to learn a group of orthogonal bases for anchors while preserving the scalability, Qiang et al. (2021) iteratively partition original data into two balanced parts using k-means++ to output informative anchors, Zhang et al. (2023) integrate anchor selection into the generation of anchor graph in which the number of connection components is the same as that of clusters to explicitly explore cluster structure, Li et al. (2024d) devise a pre-defined prior matrix for view-wise anchors to regularize their order and utilize a graph matching model to handle unpaired data, Yu et al. (2023) combine membership learning and the construction of anchors to decrease the disagreement between views, and improve the clearness of cluster grouping via trace norm regularizer, Lao et al. (2024) choose to jointly construct multiple sets of anchors for basic clusterings so as to form discriminative subspace representations.

Orthogonal to them, Xu et al. (2021b) optimize a view-common variable and view-specific variables by introducing variational auto encoder into MVC to regulate consecutive visual characteristics of multiple views, Cui et al. (2024) highlight consistent representations from the perspective of information theory and decrease the view redundancy by minimizing the representation lower bound, Zhang et al. (2022) reach to the balance between complementarity and consistency by encoding view information using an adversarial strategy and utilize a parameter-free loss to complete the formation of structured representations while avoiding over-fitting, Fu et al. (2024) excavate potential structure distributions among samples in a generative manner and utilize anchor graphs to guide the learning process by generating structured spectral embedding using graph convolution network. By virtue of tensor tool, Li et al. (2024a) orthogonally project anchor graph into a potential label space to explore the cluster distribution and alleviate the loss of spatial structure information caused by projection transformation via tensor regularization. Long et al. (2024) form an embedding tensor by stacking embedding features of all views together to simultaneously explore the inter-view and intra-view correlations, and utilize the uniformity between semantics by employing an unified constraint to guarantee the smoothness of embedding.

To enhance the block structure of anchor graph, Qin et al. (2022) integrate multiple similarity matrices into one by introducing semi-supervised information and concurrently perform self-mapping and backward encoding via reconstruction. Nie et al. (2024a) conduct number limitations on each cluster by combining min-cut and size constraints to enhance the flexibility and decrease the parameter sensitivity, and decompose lower constraints and upper constraints respectively via augmented

Lagrangian multiplier strategy. Wen et al. (2024b) enhance the robustness by reducing the negative impact of noisy features and redundant information using feature weighting constraints, and utilize graph-embedded learning to maintain the structure characteristics. Huang et al. (2022) construct various metrics by randomizing exponential similarity in metric subspace rather than original space to improve the diversification of similarity matrices, and probe into the spatial characteristics of clusters via entropy criteria. Zeng et al. (2023) capture unified semantics by eliminating the discrepancy across views using the semantically-invariant distribution hidden within views, and alleviate the impact of defective instances via distribution transformation skills. Other approaches, such as (Lu et al., 2024; Wang et al., 2021; Tang & Liu, 2022; Xu et al., 2021a; Xia et al., 2022c; Huang et al., 2024a), have been also well studied.

E Derivation Details

In this section, we provide more detailed derivation procedure about the minimization of the loss function Eq. (3).

Update $\mathbf{A}_p$: When updating $\mathbf{A}_p$, Eq. (3) equivalently becomes

$$\min_{\mathbf{A}_p} \sum_{p=1}^{v} \boldsymbol{\alpha}_p^2 \left\|\mathbf{X}_p - \mathbf{A}_p\mathbf{T}_p\mathbf{B}_p\mathbf{C}\right\|_F^2 + \lambda \left\|\mathbf{A}_p\mathbf{T}_p - \mathbf{A}_p\mathbf{T}_p\mathbf{S}_p\right\|_F^2 . \tag{17}$$

Due to the independence of views, anchor sets on different views are also independent of each other. Accordingly, we can equivalently transform Eq. (17) as

$$\min_{\mathbf{A}_p} \boldsymbol{\alpha}_p^2 \left\|\mathbf{X}_p - \mathbf{A}_p\mathbf{T}_p\mathbf{B}_p\mathbf{C}\right\|_F^2 + \lambda \left\|\mathbf{A}_p\mathbf{T}_p - \mathbf{A}_p\mathbf{T}_p\mathbf{S}_p\right\|_F^2 .$$

This is an unconstrained optimization problem, and according to the derivative value of zero, we can obtain

$$\begin{aligned} \boldsymbol{\alpha}_v^2 \left(\mathbf{A}_p\mathbf{T}_p\mathbf{B}_p\mathbf{C} - \mathbf{X}_p\right)\left(\mathbf{C}^\top\mathbf{B}_p^\top\mathbf{T}_p^\top\right) + \lambda\left(\mathbf{A}_p\mathbf{T}_p - \mathbf{A}_p\mathbf{T}_p\mathbf{S}_p\right)\left(\mathbf{T}_p^\top - \mathbf{S}_p^\top\mathbf{T}_p^\top\right) = \mathbf{0} \\ \Rightarrow \boldsymbol{\alpha}_v^2\mathbf{A}_p\mathbf{E}_p\mathbf{E}_p^\top - \boldsymbol{\alpha}_v^2\mathbf{X}_p\mathbf{E}_p^\top + \lambda\mathbf{A}_p\mathbf{F}_p\mathbf{F}_p^\top = \mathbf{0} \\ \Rightarrow \mathbf{A}_p\left(\boldsymbol{\alpha}_v^2\mathbf{E}_p\mathbf{E}_p^\top + \lambda\mathbf{F}_p\mathbf{F}_p^\top\right) = \boldsymbol{\alpha}_v^2\mathbf{X}_p\mathbf{E}_p^\top, \end{aligned} \tag{18}$$

where $\mathbf{E}_p \in \mathbb{R}^{m\times n} = \mathbf{T}_p\mathbf{B}_p\mathbf{C}$, $\mathbf{F}_p \in \mathbb{R}^{m\times m} = \mathbf{T}_p - \mathbf{T}_p\mathbf{S}_p$. $\mathbf{T}_p$ is a permutation matrix, and thus is invertible. Further, according to the property of permutation matrix that its inverse is equal to its transposition, i.e., $\mathbf{T}_p^{-1} = \mathbf{T}_p^\top$, we have that $\mathbf{T}_p^{-1}$ is also a permutation matrix, and consequently can be seen as a series of elementary transformation operations. Based on the fact that elementary transformation does not change the rank of matrix, we have $rank(\mathbf{T}_p^{-1}\mathbf{F}_p) = rank(\mathbf{F}_p)$. Additionally, $rank(\mathbf{T}_p^{-1}\mathbf{F}_p) = rank(\mathbf{I} - \mathbf{S}_p)$. Since $\mathbf{S}_p$ is an anchor self-expression matrix and its diagonal elements are zero, we have $rank(\mathbf{I} - \mathbf{S}_p) = m$. That is, its rank is full. Thus, we have $rank(\mathbf{F}_p) = m$. It is full rank and accordingly is invertible. So, $\mathbf{F}_p\mathbf{F}_p^\top$ is also invertible. Further, the eigenvalue of $\mathbf{F}_p\mathbf{F}_p^\top$ is greater than 0, the eigenvalue of $\mathbf{E}_p\mathbf{E}_p^\top$ is greater than or equal to 0, and thus the eigenvalue of $(\boldsymbol{\alpha}_v^2\mathbf{E}_p\mathbf{E}_p^\top + \lambda\mathbf{F}_p\mathbf{F}_p^\top)$ is greater than 0. Consequently, the item $\boldsymbol{\alpha}_v^2\mathbf{E}_p\mathbf{E}_p^\top + \lambda\mathbf{F}_p\mathbf{F}_p^\top$ is invertible. Based on th above analysis, we can get that $\mathbf{A}_p = \boldsymbol{\alpha}_v^2\mathbf{X}_p\mathbf{E}_p^\top\left(\boldsymbol{\alpha}_v^2\mathbf{E}_p\mathbf{E}_p^\top + \lambda\mathbf{F}_p\mathbf{F}_p^\top\right)^{-1}$.

Update $\mathbf{T}_p$: When updating $\mathbf{T}_p$, Eq. (3) equivalently becomes

$$\begin{aligned} \min_{\mathbf{T}_p} \sum_{p=1}^{v} \boldsymbol{\alpha}_p^2 \left\|\mathbf{X}_p - \mathbf{A}_p\mathbf{T}_p\mathbf{B}_p\mathbf{C}\right\|_F^2 + \lambda \left\|\mathbf{A}_p\mathbf{T}_p - \mathbf{A}_p\mathbf{T}_p\mathbf{S}_p\right\|_F^2 \\ \text{s.t. } \mathbf{T}_p^\top\mathbf{1} = \mathbf{1}, \mathbf{T}_p\mathbf{1} = \mathbf{1}, \mathbf{T}_p \in \{0,1\}^{m\times m}. \end{aligned} \tag{19}$$

Due to $\mathbf{T}_p$ being performed on respective view, we can separately optimize each $\mathbf{T}_p$. Thus, Eq. (19) can be equivalently written as

$$\begin{aligned} \min_{\mathbf{T}_p} \boldsymbol{\alpha}_p^2 \left\|\mathbf{X}_p - \mathbf{A}_p\mathbf{T}_p\mathbf{B}_p\mathbf{C}\right\|_F^2 + \lambda \left\|\mathbf{A}_p\mathbf{T}_p - \mathbf{A}_p\mathbf{T}_p\mathbf{S}_p\right\|_F^2 \\ \text{s.t. } \mathbf{T}_p^\top\mathbf{1} = \mathbf{1}, \mathbf{T}_p\mathbf{1} = \mathbf{1}, \mathbf{T}_p \in \{0,1\}^{m\times m}. \end{aligned}$$

After expanding the objective using the trace operation and deleting irrelevant items, we can get

$$
\begin{aligned}
&\min_{\mathbf{T}_p} \boldsymbol{\alpha}_p^2 \left\| \mathbf{X}_p - \mathbf{A}_p \mathbf{T}_p \mathbf{B}_p \mathbf{C} \right\|_F^2 + \lambda \left\| \mathbf{A}_p \mathbf{T}_p - \mathbf{A}_p \mathbf{T}_p \mathbf{S}_p \right\|_F^2 \\
\Rightarrow &\min_{\mathbf{T}_p} \operatorname{Tr}\left(\boldsymbol{\alpha}_p^2 \mathbf{A}_p \mathbf{T}_p \mathbf{B}_p \mathbf{C}\mathbf{C}^\top \mathbf{B}_p^\top \mathbf{T}_p^\top \mathbf{A}_p^\top - 2\boldsymbol{\alpha}_p^2 \mathbf{A}_p^\top \mathbf{X}_p \mathbf{C}^\top \mathbf{B}_p^\top \mathbf{T}_p^\top + \lambda \mathbf{A}_p \mathbf{T}_p \mathbf{T}_p^\top \mathbf{A}_p^\top + \right. \\
&\left. \lambda \mathbf{A}_p \mathbf{T}_p \mathbf{S}_p \mathbf{S}_p^\top \mathbf{T}_p^\top \mathbf{A}_p^\top - 2\lambda \mathbf{A}_p \mathbf{T}_p \mathbf{S}_p^\top \mathbf{T}_p^\top \mathbf{A}_p^\top \right).
\end{aligned} \tag{20}
$$

According to the fact that $\mathbf{T}_p$ is a permutation matrix, we have $\mathbf{T}_p\mathbf{T}_p^\top = \mathbf{I}$. Additionally, considering that $\sum_{i=1}^{k} \mathbf{C}_{i,j} = 1, j \in \{1, 2, \ldots, n\}, \mathbf{C} \in \{0, 1\}^{k \times n}$, we have that $\mathbf{C}\mathbf{C}^\top$ is a diagonal matrix, and its diagonal elements are $\sum_{j=1}^{n} \mathbf{C}_{i,j}$, $i = 1, 2, \cdots k$. Further, combined with $\mathbf{B}_p$ being orthogonal, we can obtain $\operatorname{Tr}\left(\mathbf{B}_p \mathbf{C}\mathbf{C}^\top \mathbf{B}_p^\top\right) = \operatorname{Tr}\left(\mathbf{C}\mathbf{C}^\top\right) = \sum_{i,j} \mathbf{C}_{i,j}$. Based on these analysis, we can get

$$
\begin{aligned}
&\min_{\mathbf{T}_p} \boldsymbol{\alpha}_p^2 \left\| \mathbf{X}_p - \mathbf{A}_p \mathbf{T}_p \mathbf{B}_p \mathbf{C} \right\|_F^2 + \lambda \left\| \mathbf{A}_p \mathbf{T}_p - \mathbf{A}_p \mathbf{T}_p \mathbf{S}_p \right\|_F^2 \\
\Rightarrow &\min_{\mathbf{T}_p} \operatorname{Tr}\left(-2\boldsymbol{\alpha}_p^2 \mathbf{T}_p^\top \mathbf{A}_p^\top \mathbf{X}_p \mathbf{C}^\top \mathbf{B}_p^\top + \lambda \mathbf{T}_p^\top \mathbf{A}_p^\top \mathbf{A}_p \mathbf{T}_p \mathbf{S}_p \mathbf{S}_p^\top + \right. \\
&\left. \boldsymbol{\alpha}_p^2 \mathbf{T}_p^\top \mathbf{A}_p^\top \mathbf{A}_p \mathbf{T}_p \mathbf{B}_p \mathbf{C}\mathbf{C}^\top \mathbf{B}_p^\top - 2\lambda \mathbf{T}_p^\top \mathbf{A}_p^\top \mathbf{A}_p \mathbf{T}_p \mathbf{S}_p^\top \right) \\
\Rightarrow &\min_{\mathbf{T}_p} \operatorname{Tr}\left(\lambda \mathbf{T}_p^\top \mathbf{G}_p \mathbf{T}_p \mathbf{H}_p + \boldsymbol{\alpha}_p^2 \mathbf{T}_p^\top \mathbf{G}_p \mathbf{T}_p \mathbf{M}_p - 2\lambda \mathbf{T}_p^\top \mathbf{G}_p \mathbf{T}_p \mathbf{S}_p^\top - 2\boldsymbol{\alpha}_p^2 \mathbf{T}_p^\top \mathbf{J}_p \right) \\
\Rightarrow &\min_{\mathbf{T}_p} \operatorname{Tr}\left(\mathbf{T}_p^\top \mathbf{G}_p \mathbf{T}_p \left(\lambda \mathbf{H}_p + \boldsymbol{\alpha}_p^2 \mathbf{M}_p \right) - 2\lambda \mathbf{T}_p^\top \mathbf{G}_p \mathbf{T}_p \mathbf{S}_p^\top - 2\boldsymbol{\alpha}_p^2 \mathbf{T}_p^\top \mathbf{J}_p \right),
\end{aligned} \tag{21}
$$

where $\mathbf{G}_p \in \mathbb{R}^{m \times m} = \mathbf{A}_p^\top \mathbf{A}_p$, $\mathbf{H}_p \in \mathbb{R}^{m \times m} = \mathbf{S}_p \mathbf{S}_p^\top$, $\mathbf{M}_p \in \mathbb{R}^{m \times m} = \mathbf{B}_p \mathbf{C}\mathbf{C}^\top \mathbf{B}_p^\top$, $\mathbf{J}_p \in \mathbb{R}^{m \times m} = \mathbf{A}_p^\top \mathbf{X}_p \mathbf{C}^\top \mathbf{B}_p^\top$. Combined with the feasible region in Eq. 19, we can determine the optimal solution of $\mathbf{T}_p$ via traversal searching using $[\mathbf{e}_1, \mathbf{e}_2, \cdots, \mathbf{e}_i, \cdots, \mathbf{e}_m]$ where $\mathbf{e}_i$ is the one-hot vector. Kindly note that the size of $\mathbf{T}_p$ is $m \times m$ and m is generally small, performing traversal searching on $\mathbf{T}_p$ will not incur significant computing costs.

Update $\mathbf{B}_p$: When updating $\mathbf{B}_p$, Eq. (3) equivalently becomes

$$
\begin{aligned}
&\min_{\mathbf{B}_p} \sum_{p=1}^{v} \boldsymbol{\alpha}_p^2 \left\| \mathbf{X}_p - \mathbf{A}_p \mathbf{T}_p \mathbf{B}_p \mathbf{C} \right\|_F^2 + \beta \operatorname{Tr}(\mathbf{B}_p^\top \mathbf{L}_\mathbf{s} \mathbf{B}_p \mathbf{C}\mathbf{C}^\top) \\
&\text{s.t. } \mathbf{B}_p^\top \mathbf{B}_p = \mathbf{I}_k.
\end{aligned} \tag{22}
$$

Since the basic coefficient matrices $\{\mathbf{B}_p\}_{p=1}^{v}$ on different views are independent of each other, we can equivalently transform Eq. (22) as

$$
\begin{aligned}
&\min_{\mathbf{B}_p} \boldsymbol{\alpha}_p^2 \left\| \mathbf{X}_p - \mathbf{A}_p \mathbf{T}_p \mathbf{B}_p \mathbf{C} \right\|_F^2 + \beta \operatorname{Tr}(\mathbf{B}_p^\top \mathbf{L}_\mathbf{s} \mathbf{B}_p \mathbf{C}\mathbf{C}^\top) \\
&\text{s.t. } \mathbf{B}_p^\top \mathbf{B}_p = \mathbf{I}_k.
\end{aligned} \tag{23}
$$

Expanding the objective and then deleting irrelevant items, we can obtain

$$
\begin{aligned}
&\min_{\mathbf{B}_p} \boldsymbol{\alpha}_p^2 \left\| \mathbf{X}_p - \mathbf{A}_p \mathbf{T}_p \mathbf{B}_p \mathbf{C} \right\|_F^2 + \beta \operatorname{Tr}(\mathbf{B}_p^\top \mathbf{L}_\mathbf{s} \mathbf{B}_p \mathbf{C}\mathbf{C}^\top) \\
\Rightarrow &\min_{\mathbf{B}_p} \operatorname{Tr}\left(\boldsymbol{\alpha}_p^2 \mathbf{A}_p \mathbf{T}_p \mathbf{B}_p \mathbf{C}\mathbf{C}^\top \mathbf{B}_p^\top \mathbf{T}_p^\top \mathbf{A}_p^\top - 2\boldsymbol{\alpha}_p^2 \mathbf{T}_p^\top \mathbf{A}_p^\top \mathbf{X}_p \mathbf{C}^\top \mathbf{B}_p^\top + \beta \mathbf{B}_p^\top \mathbf{L}_\mathbf{s} \mathbf{B}_p \mathbf{C}\mathbf{C}^\top \right)
\end{aligned} \tag{24}
$$

Since $\mathbf{C}\mathbf{C}^\top$ is diagonal and $\mathbf{B}_p$ is orthogonal, we can further have

$$
\begin{aligned}
&\min_{\mathbf{B}_p} \boldsymbol{\alpha}_p^2 \left\| \mathbf{X}_p - \mathbf{A}_p \mathbf{T}_p \mathbf{B}_p \mathbf{C} \right\|_F^2 + \beta \operatorname{Tr}(\mathbf{B}_p^\top \mathbf{L}_\mathbf{s} \mathbf{B}_p \mathbf{C}\mathbf{C}^\top) \\
\Rightarrow &\min_{\mathbf{B}_p} \operatorname{Tr}\left(\beta \mathbf{B}_p^\top \mathbf{L}_\mathbf{s} \mathbf{B}_p \mathbf{C}\mathbf{C}^\top + \boldsymbol{\alpha}_p^2 \mathbf{B}_p^\top \mathbf{Q}_p \mathbf{B}_p \mathbf{C}\mathbf{C}^\top - 2\boldsymbol{\alpha}_p^2 \mathbf{T}_p^\top \mathbf{A}_p^\top \mathbf{X}_p \mathbf{C}^\top \mathbf{B}_p^\top \right) \\
\Rightarrow &\min_{\mathbf{B}_p} \operatorname{Tr}\left(\mathbf{B}_p^\top \left(\beta \mathbf{L}_\mathbf{s} + \boldsymbol{\alpha}_p^2 \mathbf{Q}_p \right) \mathbf{B}_p \mathbf{C}\mathbf{C}^\top - 2\boldsymbol{\alpha}_p^2 \mathbf{C} \mathbf{X}_p^\top \mathbf{A}_p \mathbf{T}_p \mathbf{B}_p \right),
\end{aligned} \tag{25}
$$

where $\mathbf{Q}_p \in \mathbb{R}^{m \times m} = \mathbf{T}_p^\top \mathbf{A}_p^\top \mathbf{A}_p \mathbf{T}_p$.

Considering that the feasible region $\mathbf{B}_p^\top \mathbf{B}_p = \mathbf{I}_k$ can be equivalently divided into $[\mathbf{B}_p]_{:,j}^\top [\mathbf{B}_p]_{:,j} = 1$ and $[\mathbf{B}_p]_{:,j}^\top [\mathbf{B}_p]_{:,i} = 0, i = 1, 2, \cdots, k, i \neq j, j = 1, 2, \cdots, k$, we can solve $\mathbf{B}_p$ column by column. Thus, we have

$$
\begin{aligned}
&\min_{\mathbf{B}_p} \operatorname{Tr}\left(\mathbf{B}_p^\top \left(\beta \mathbf{L}_\mathbf{s} + \boldsymbol{\alpha}_p^2 \mathbf{Q}_p\right) \mathbf{B}_p \mathbf{C}\mathbf{C}^\top - 2\boldsymbol{\alpha}_p^2 \mathbf{C}\mathbf{X}_p^\top \mathbf{A}_p \mathbf{T}_p \mathbf{B}_p\right) \\
\Rightarrow &\min_{[\mathbf{B}_p]_{:,j}} [\mathbf{B}_p^\top]_{j,:} \left(\beta \mathbf{L}_\mathbf{s} + \boldsymbol{\alpha}_p^2 \mathbf{Q}_p\right) \mathbf{B}_p [\mathbf{C}\mathbf{C}^\top]_{:,j} + \left[-2\boldsymbol{\alpha}_p^2 \mathbf{C}\mathbf{X}_p^\top \mathbf{A}_p \mathbf{T}_p\right]_{j,:} [\mathbf{B}_p]_{:,j} \\
\Rightarrow &\min_{[\mathbf{B}_p]_{:,j}} [\mathbf{B}_p]_{:,j}^\top \sum_{i=1}^{n} \mathbf{C}_{j,i} \left(\beta \mathbf{L}_\mathbf{s} + \boldsymbol{\alpha}_p^2 \mathbf{Q}_p\right) [\mathbf{B}_p]_{:,j} + \left[-2\boldsymbol{\alpha}_p^2 \mathbf{C}\mathbf{X}_p^\top \mathbf{A}_p \mathbf{T}_p\right]_{j,:} [\mathbf{B}_p]_{:,j},
\end{aligned}
\tag{26}
$$

where the objective is quadratic. Besides, the constraint $[\mathbf{B}_p]_{:,j}^\top [\mathbf{B}_p]_{:,j} = 1$ can be equivalently written as $[\mathbf{B}_p]_{:,j}^\top \mathbf{I}_{m\times m} [\mathbf{B}_p]_{:,j} - 1 = 0$. $[\mathbf{B}_p]_{:,j}^\top [\mathbf{B}_p]_{:,i} = 0, i = 1, 2, \cdots, k, i \neq j$ can be written as $\left[[\mathbf{B}_p]_{:,1}, [\mathbf{B}_p]_{:,2}, \cdots, [\mathbf{B}_p]_{:,j-1}, [\mathbf{B}_p]_{:,j+1}, \cdots, [\mathbf{B}_p]_{:,k}\right]^\top [\mathbf{B}_p]_{:,j} = \mathbf{0}_{(k-1)\times 1}$. Apparently, the constraints are also quadratic. Consequently, the optimization problem about $\mathbf{B}_p$ can be equivalently transformed as

$$
\begin{aligned}
&\min_{[\mathbf{B}_p]_{:,j}} [\mathbf{B}_p]_{:,j}^\top \sum_{i=1}^{n} \mathbf{C}_{j,i} \left(\beta \mathbf{L}_\mathbf{s} + \boldsymbol{\alpha}_p^2 \mathbf{Q}_p\right) [\mathbf{B}_p]_{:,j} + \left[-2\boldsymbol{\alpha}_p^2 \mathbf{C}\mathbf{X}_p^\top \mathbf{A}_p \mathbf{T}_p\right]_{j,:} [\mathbf{B}_p]_{:,j} \\
&\text{s.t. } [\mathbf{B}_p]_{:,j}^\top \mathbf{I}_{m\times m} [\mathbf{B}_p]_{:,j} - 1 = 0, \\
&\left[[\mathbf{B}_p]_{:,1}, [\mathbf{B}_p]_{:,2}, \cdots, [\mathbf{B}_p]_{:,j-1}, [\mathbf{B}_p]_{:,j+1}, \cdots, [\mathbf{B}_p]_{:,k}\right]^\top [\mathbf{B}_p]_{:,j} = \mathbf{0}_{(k-1)\times 1}.
\end{aligned}
$$

This is a QCQP optimization problem, and can be solved in $\mathcal{O}(m^3)$ computing complexity.

Update $\mathbf{S}_p$: When updating $\mathbf{S}_p$, Eq. (3) equivalently becomes

$$
\begin{aligned}
&\min_{\mathbf{S}_p} \lambda \left\|\mathbf{A}_p \mathbf{T}_p - \mathbf{A}_p \mathbf{T}_p \mathbf{S}_p\right\|_F^2 + \beta \operatorname{Tr}(\mathbf{B}_p^\top \mathbf{L}_\mathbf{s} \mathbf{B}_p \mathbf{C}\mathbf{C}^\top) \\
&\text{s.t. } \mathbf{S}_p^\top \mathbf{1} = \mathbf{1}, \mathbf{S}_p \geq 0, \sum_{i=1}^{m} [\mathbf{S}_p]_{i,i} = 0.
\end{aligned}
\tag{27}
$$

Expanding the objective, we have

$$
\begin{aligned}
&\min_{\mathbf{S}_p} \lambda \left\|\mathbf{A}_p \mathbf{T}_p - \mathbf{A}_p \mathbf{T}_p \mathbf{S}_p\right\|_F^2 + \beta \operatorname{Tr}(\mathbf{B}_p^\top \mathbf{L}_\mathbf{s} \mathbf{B}_p \mathbf{C}\mathbf{C}^\top) \\
\Rightarrow &\min_{\mathbf{S}_p} \operatorname{Tr}\left(\lambda \mathbf{A}_p \mathbf{T}_p \mathbf{S}_p \mathbf{S}_p^\top \mathbf{T}_p^\top \mathbf{A}_p^\top - 2\lambda \mathbf{A}_p \mathbf{T}_p \mathbf{S}_p^\top \mathbf{T}_p^\top \mathbf{A}_p^\top \right. \\
&\left. + \lambda \mathbf{A}_p \mathbf{T}_p \mathbf{T}_p^\top \mathbf{A}_p^\top + \beta \mathbf{B}_p^\top \mathbf{D}_p \mathbf{B}_p \mathbf{C}\mathbf{C}^\top - \beta \mathbf{B}_p^\top \mathbf{S}_p \mathbf{B}_p \mathbf{C}\mathbf{C}^\top\right) \\
\Rightarrow &\min_{\mathbf{S}_p} \operatorname{Tr}\left(\lambda \mathbf{A}_p \mathbf{T}_p \mathbf{S}_p \mathbf{S}_p^\top \mathbf{T}_p^\top \mathbf{A}_p^\top - 2\lambda \mathbf{A}_p \mathbf{T}_p \mathbf{S}_p^\top \mathbf{T}_p^\top \mathbf{A}_p^\top - \beta \mathbf{B}_p^\top \mathbf{S}_p \mathbf{B}_p \mathbf{C}\mathbf{C}^\top\right) \\
\Rightarrow &\min_{\mathbf{S}_p} \operatorname{Tr}\left(\lambda \mathbf{S}_p^\top \mathbf{T}_p^\top \mathbf{A}_p^\top \mathbf{A}_p \mathbf{T}_p \mathbf{S}_p - 2\lambda \mathbf{T}_p^\top \mathbf{A}_p^\top \mathbf{A}_p \mathbf{T}_p \mathbf{S}_p - \beta \mathbf{B}_p \mathbf{C}\mathbf{C}^\top \mathbf{B}_p^\top \mathbf{S}_p\right) \\
\Rightarrow &\min_{\mathbf{S}_p} \operatorname{Tr}\left(\lambda \mathbf{S}_p^\top \mathbf{Q}_p \mathbf{S}_p - 2\lambda \mathbf{Q}_p \mathbf{S}_p - \beta \mathbf{M}_p \mathbf{S}_p\right) \\
\Rightarrow &\min_{\mathbf{S}_p} \operatorname{Tr}\left(\mathbf{S}_p^\top \mathbf{Q}_p \mathbf{S}_p + 2\left(-\mathbf{Q}_p - \frac{\beta}{2\lambda}\mathbf{M}_p\right) \mathbf{S}_p\right),
\end{aligned}
\tag{28}
$$

where $\mathbf{Q}_p \in \mathbb{R}^{m\times m} = \mathbf{T}_p^\top \mathbf{A}_p^\top \mathbf{A}_p \mathbf{T}_p$, $\mathbf{M}_p \in \mathbb{R}^{m\times m} = \mathbf{B}_p \mathbf{C}\mathbf{C}^\top \mathbf{B}_p^\top$.

Noticed that the feasible region is for each column of $\mathbf{S}_p$, consequently, we can equivalently rewrite the constraints in the form of columns. That is, we can transform $\mathbf{S}_p^\top \mathbf{1} = \mathbf{1}, \mathbf{S}_p \geq 0, \sum_{i=1}^{m} [\mathbf{S}_p]_{i,i} = 0$ as $[\mathbf{S}_p]_{:,j}^\top \mathbf{1} = 1, [\mathbf{S}_p]_{:,j} \geq 0, [\mathbf{S}_p]_{j,j} = 0, j = 1, 2, \cdots, m$. Further, we can transform $[\mathbf{S}_p]_{j,j} = 0, j = 1, 2, \cdots, m$ as $\mathbf{e}_j^\top [\mathbf{S}_p]_{:,j} = 0, j = 1, 2, \cdots, m$, where $\mathbf{e}_j$ is the one-hot vector.

Based on these, for the objective function, we can further have

$$
\begin{aligned}
&\min_{\mathbf{S}_p} \operatorname{Tr}\left(\mathbf{S}_p^\top \mathbf{Q}_p \mathbf{S}_p + 2\left(-\mathbf{Q}_p - \frac{\beta}{2\lambda}\mathbf{M}_p\right) \mathbf{S}_p\right) \\
\Rightarrow &\min_{[\mathbf{S}_p]_{:,j}} \frac{1}{2} [\mathbf{S}_p]_{:,j}^\top \mathbf{Q}_p [\mathbf{S}_p]_{:,j} + \left(-\mathbf{Q}_p - \frac{\beta}{2\lambda}\mathbf{M}_p\right)_{j,:} [\mathbf{S}_p]_{:,j}.
\end{aligned}
\tag{29}
$$

Therefore, the optimization problem about $\mathbf{S}_p$ can be equivalently written as

$$\begin{aligned} \min_{[\mathbf{S}_p]_{:,j}} \frac{1}{2}[\mathbf{S}_p]_{:,j}^\top \mathbf{Q}_p [\mathbf{S}_p]_{:,j} + \left(-\mathbf{Q}_p - \frac{\beta}{2\lambda}\mathbf{M}_p\right)_{j,:} [\mathbf{S}_p]_{:,j} \\ \text{s.t. } [\mathbf{S}_p]_{:,j}^\top \mathbf{1} = 1, 0 \leq [\mathbf{S}_p]_{:,j}, \mathbf{e}_j^\top [\mathbf{S}_p]_{:,j} = 0, j = 1, 2, \cdots, m, \end{aligned} \tag{30}$$

which is a QP problem, and can be solved within $\mathcal{O}(m^2)$ computing complexity.

Update $\mathbf{C}$: When updating $\mathbf{C}$, Eq. (3) equivalently becomes

$$\begin{aligned} \min_{\mathbf{C}} \sum_{p=1}^{v} \boldsymbol{\alpha}_p^2 \left\|\mathbf{X}_p - \mathbf{A}_p\mathbf{T}_p\mathbf{B}_p\mathbf{C}\right\|_F^2 + \beta \operatorname{Tr}(\mathbf{B}_p^\top \mathbf{L}_\mathbf{s} \mathbf{B}_p \mathbf{C}\mathbf{C}^\top) \\ \text{s.t. } \sum_{i=1}^{k} \mathbf{C}_{i,j} = 1, j = 1, 2, \ldots, n, \mathbf{C} \in \{0, 1\}^{k \times n}. \end{aligned} \tag{31}$$

For the objective function, we have

$$\begin{aligned} &\min_{\mathbf{C}} \sum_{p=1}^{v} \boldsymbol{\alpha}_p^2 \left\|\mathbf{X}_p - \mathbf{A}_p\mathbf{T}_p\mathbf{B}_p\mathbf{C}\right\|_F^2 + \beta \operatorname{Tr}(\mathbf{B}_p^\top \mathbf{L}_\mathbf{s} \mathbf{B}_p \mathbf{C}\mathbf{C}^\top) \\ \Rightarrow &\min_{\mathbf{C}} \operatorname{Tr}\left(\mathbf{C}^\top \sum_{p=1}^{v} \boldsymbol{\alpha}_p^2 \mathbf{B}_p^\top \mathbf{T}_p^\top \mathbf{A}_p^\top \mathbf{A}_p \mathbf{T}_p \mathbf{B}_p \mathbf{C} - 2\sum_{p=1}^{v} \boldsymbol{\alpha}_p^2 \mathbf{X}_p^\top \mathbf{A}_p \mathbf{T}_p \mathbf{B}_p \mathbf{C} + \beta \mathbf{C}^\top \sum_{p=1}^{v} \mathbf{B}_p^\top \mathbf{L}_\mathbf{s} \mathbf{B}_p \mathbf{C}\right) \\ \Rightarrow &\min_{\mathbf{C}} \operatorname{Tr}\left(\mathbf{C}^\top \left(\sum_{p=1}^{v} \boldsymbol{\alpha}_p^2 \mathbf{B}_p^\top \mathbf{T}_p^\top \mathbf{A}_p^\top \mathbf{A}_p \mathbf{T}_p \mathbf{B}_p + \beta \mathbf{B}_p^\top \mathbf{L}_\mathbf{s} \mathbf{B}_p\right) \mathbf{C} - 2\sum_{p=1}^{v} \boldsymbol{\alpha}_p^2 \mathbf{X}_p^\top \mathbf{A}_p \mathbf{T}_p \mathbf{B}_p \mathbf{C}\right) \\ \Rightarrow &\min_{\mathbf{C}} \operatorname{Tr}\left(\mathbf{C}^\top \mathbf{W} \mathbf{C} - \mathbf{Z}\mathbf{C}\right), \end{aligned} \tag{32}$$

where $\mathbf{W} \in \mathbb{R}^{k \times k} = \sum_{p=1}^{v} \boldsymbol{\alpha}_p^2 \mathbf{B}_p^\top \mathbf{T}_p^\top \mathbf{A}_p^\top \mathbf{A}_p \mathbf{T}_p \mathbf{B}_p + \beta \mathbf{B}_p^\top \mathbf{L}_\mathbf{s} \mathbf{B}_p$, $\mathbf{Z} \in \mathbb{R}^{n \times k} = 2\sum_{p=1}^{v} \boldsymbol{\alpha}_p^2 \mathbf{X}_p^\top \mathbf{A}_p \mathbf{T}_p \mathbf{B}_p$.

The constraints mean that there is only one non-zero element in each column of $\mathbf{C}$, and consequently we can optimize $\mathbf{C}$ by column. We can get

$$\min_{\mathbf{C}} \operatorname{Tr}\left(\mathbf{C}^\top \mathbf{W} \mathbf{C} - \mathbf{Z}\mathbf{C}\right) \Rightarrow \min_{\mathbf{C}_{:,j}} \mathbf{C}_{:,j}^\top \mathbf{W} \mathbf{C}_{:,j} - \mathbf{Z}_{j,:} \mathbf{C}_{:,j}. \tag{33}$$

Further, the item $\mathbf{C}_{:,j}^\top \mathbf{W} \mathbf{C}_{:,j}$ indicates that it takes a diagonal element of $\mathbf{W}$, and $\mathbf{Z}_{j,:}\mathbf{C}_{:,j}$ indicates that it takes a element of $\mathbf{Z}_{j,:}$. Thus, we can determine the corresponding index of minimum by

$$l^* = \arg\min_{l} \mathbf{W}_{l,l} - \mathbf{Z}_{j,l}, \quad l = 1, 2, \cdots, k. \tag{34}$$

Then, the value of $\mathbf{C}_{:,j}$ can be determined by assigning $\mathbf{C}_{l^*,j}$ as 1 while assigning other elements of $\mathbf{C}_{:,j}$ as 0.

Update $\boldsymbol{\alpha}$: When updating $\boldsymbol{\alpha}$, Eq. (3) equivalently becomes

$$\begin{aligned} \min_{\boldsymbol{\alpha}} \sum_{p=1}^{v} \boldsymbol{\alpha}_p^2 \left\|\mathbf{X}_p - \mathbf{A}_p\mathbf{T}_p\mathbf{B}_p\mathbf{C}\right\|_F^2 \\ \text{s.t. } \boldsymbol{\alpha}^\top \mathbf{1} = 1, \boldsymbol{\alpha} \geq 0. \end{aligned}$$

Considering that the term $\frac{1}{b_p} = \left\|\mathbf{X}_p - \mathbf{A}_p\mathbf{T}_p\mathbf{B}_p\mathbf{C}\right\|_F^2$ is a constant with respect to $\boldsymbol{\alpha}$, we can solve $\boldsymbol{\alpha}$ using Cauchy inequality. Specially, we can get that the optimal solution is $\boldsymbol{\alpha}_p = \frac{b_p}{\sum_{p=1}^{v} b_p}$.

F More Conclusions for Table 1

1. On CALTE7, MFLVC receives better clustering results in NMI, probably because it achieves reconstruction and consistency by learning features at multiple levels rather than at single level for each view, and utilizes the consensus semantics shared in all views and semantic labels to decrease the view-private unfavorable influence.

2. FPMVS achieves 0.29% increasement in terms of ACC on CIF10Tra4, and possible reasons are that it employs a group of projectors to maintain the anchor dimension consistency and extracts consensus multi-view isomeric features by utilizing an unified graph structure with cluster distribution constraints.
3. On Cora in Fscore, MSCIAS slightly surpasses us with 0.72%, which is mainly because it enforces encoded similarity to maximally depend on the potential intact-samples through HSIC criterion and utilizes the local connectivity of intact space to eliminate outliers and enhance the distinguishability of similarity.
4. For SFMC, it makes preferable results on REU7200 in NMI, main reasons of which could be that it integrates connectivity constraint into the learning of joint graph to reflect cluster distribution and adaptively adjusts the graph contributions on different views in self-supervised weighting way.

G Additional Ablation Study

In the paper, rather than treating views equally, we adopt a square weighting scheme to adaptively combine views together. To validate the effectiveness of this strategy, we conduct the comparison experiments with equal view weighting (EVW). The results are summarized in Table 6, where AVW denotes the clustering results based on our adaptive view weighting. Obviously, AVW receives more desirable results than EVW in most cases, which suggests that the adaptive view weighting strategy is recommendable. Additionally, we also plot the learned view weights, as shown in Fig. 3. It can be seen that it indeed assigns different weights to measure the contribution between views.

Table 6: The effectiveness of view weighting

Metric	Ablation	DERMATO	CALTE7	Cora	REU7200	Reuters	CIF10Tra4	FasMNI4V
NMI	EVW	89.44	42.88	33.06	3.60	29.54	15.20	56.84
	AVW	**89.97**	**45.25**	**43.70**	**6.25**	**31.87**	**15.64**	**59.21**
ACC	EVW	84.59	76.73	44.94	16.82	47.84	25.26	52.69
	AVW	**85.47**	**80.66**	**52.44**	**26.22**	**54.26**	**26.83**	**57.36**
Fscore	EVW	86.59	71.80	35.36	**28.77**	42.32	18.03	46.90
	AVW	**87.92**	**78.12**	**41.12**	28.55	**44.84**	**20.64**	**51.37**

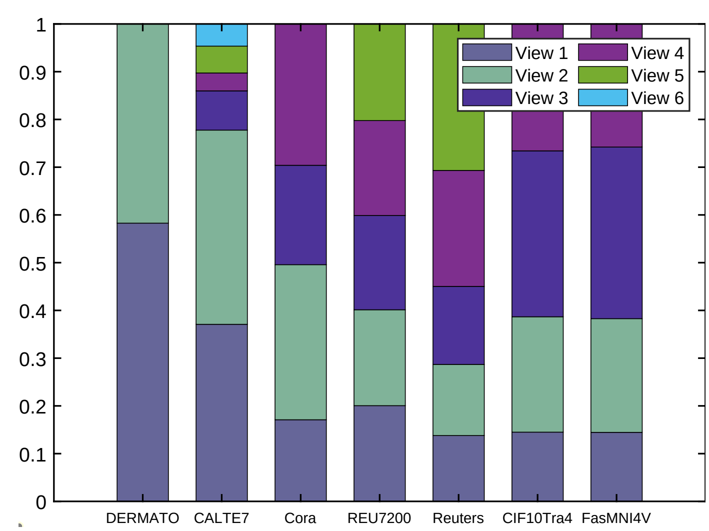

Figure 3: The learned view weights on seven public datasets.

Besides, unlike current techniques generating anchors via random sampling or heuristic searching, which leads to anchors being separated from subsequent procedures like graph learning and spectral construction, we integrate anchors into objective optimization framework to make them able to interactive with other parts and thereby facilitate each other. To investigate its effectiveness, we organize corresponding ablation experiment and present the comparison results in Table 7, where HS denotes the clustering results based on anchors generated by heuristic searching while LA denotes the results based on our anchor learning. It is easy to observe that LA outperforms HS with noticeable margins, which illustrates that the anchor learning strategy is functional and can provide more pleasing clustering results.

Table 7: The effectiveness of anchor learning

Metric	Ablation	DERMATO	CALTE7	Cora	REU7200	Reuters	CIF10Tra4	FasMNI4V
NMI	HS	69.84	37.95	33.54	1.06	1.43	12.98	47.07
	LA	**89.97**	**45.25**	**43.70**	**6.25**	**31.87**	**15.64**	**59.21**
ACC	HS	65.64	64.59	30.24	16.68	27.20	24.08	47.21
	LA	**85.47**	**80.66**	**52.44**	**26.22**	**54.26**	**26.83**	**57.36**
Fscore	HS	69.33	61.54	30.40	24.43	35.25	18.03	41.43
	LA	**87.92**	**78.12**	**41.12**	**28.55**	**44.84**	**20.64**	**51.37**

H Single-view Scenario Comparison

Except for multi-view scenarios, sometimes we also may encounter the datasets containing only one view. To validate the ability to tackle single view scenarios, we conduct clustering operation on one view rather than on all views of datasets mentioned earlier. The experimental results are summarized in Table 8, 9 and 10. From these tables, we can draw that ADAGE, MELVC, OrthNTF and FMVACC are powerless against single view scenarios, which is mainly because they generally need utilize the information of other views to help optimize. FMR, PMSC, AMGL, MSCIAS, MVSC, etc, are able to work properly with single view scenarios, nevertheless, they generally produce inferior clustering results in most situations. By comparison, besides being able to operate properly on single view scenarios, our DLA-EF-JA also can generate desirable results. Accordingly, our DLA-EF-JA enjoys wider serviceability.

Table 8: Single-view experimental results in NMI

Dataset	DERMATO	CALTE7	Cora	REU7200	Reuters	CIF10Tra4	FasMNI4V
FMR	76.63(±3.98)	1.38(±0.18)	5.12(±0.17)	-	-	-	-
PMSC	80.21(±5.10)	34.04(±0.71)	6.12(±0.83)	1.43(±0.12)	-	-	-
AMGL	3.07(±0.24)	34.34(±1.28)	0.83(±0.02)	0.72(±0.09)	0.89(±0.03)	-	-
MSCIAS	75.79(±4.77)	35.42(±1.66)	9.45(±0.46)	1.69(±0.27)	1.22(±0.17)	-	-
MVSC	52.19(±11.98)	25.22(±1.25)	-	-	-	-	-
MLRSSC	0.54(±0.00)	0.73(±0.00)	0.48(±0.00)	0.56(±0.00)	-	-	-
MPAC	77.69(±0.00)	29.88(±0.00)	9.30(±0.00)	1.29(±0.00)	-	-	-
MCLES	78.19(±3.49)	27.64(±1.87)	8.47(±0.93)	-	-	-	-
FMCNOF	42.62(±4.32)	9.42(±1.23)	4.58(±0.79)	1.11(±0.17)	-	9.36(±2.32)	32.07(±3.26)
ADAGAE	-	-	-	-	-	-	-
PFSC	76.00(±2.45)	32.47(±1.85)	-	-	-	-	-
SFMC	62.77(±0.00)	27.46(±0.00)	6.01(±0.00)	2.37(±0.00)	1.44(±0.00)	9.44(±0.00)	-
MSGL	10.33(±0.74)	-	-	1.15(±0.08)	1.02(±0.06)	7.64(±0.68)	-
FPMVS	77.14(±5.56)	34.02(±1.85)	9.28(±1.64)	2.44(±0.24)	**11.73(±3.38)**	10.99(±0.82)	53.71(±2.18)
MFLVC	-	-	-	-	-	-	-
UOMVSC	77.83(±0.00)	28.86(±0.00)	8.95(±0.00)	2.83(±0.00)	9.45(±0.00)	-	-
PGSC	69.96(±4.66)	22.46(±2.37)	1.43(±0.32)	2.03(±0.26)	0.92(±0.08)	-	-
OrthNTF	-	-	-	-	-	-	-
FMVACC	-	-	-	-	-	-	-
FASTMI	78.85(±2.10)	32.49(±1.29)	9.77(±2.13)	**3.03(±0.66)**	10.12(±1.58)	13.48(±0.64)	58.14(±1.73)
Ours	**80.52(±0.00)**	**36.59(±0.00)**	**10.04(±0.00)**	2.50(±0.00)	1.37(±0.00)	**15.09(±0.00)**	**61.44(±0.00)**

I Effectiveness in Gathering Multi-view Information

Compared to single view datasets, multi-view data can provide more comprehensive and detailed descriptions for the same instance and thereby facilitates more accurate representations for better

Table 9: Single-view experimental results in ACC

Dataset	DERMATO	CALTE7	Cora	REU7200	Reuters	CIF10Tra4	FasMNI4V
FMR	66.50(±5.19)	21.59(±0.49)	24.08(±0.38)	-	-	-	-
PMSC	64.83(±8.99)	38.18(±1.81)	27.93(±0.86)	19.24(±0.53)	-	-	-
AMGL	22.09(±0.16)	39.72(±1.35)	14.67(±0.17)	17.00(±0.05)	20.32(±0.27)	-	-
MSCIAS	64.35(±8.27)	40.63(±2.93)	30.88(±1.30)	19.25(±0.93)	25.38(±1.44)	-	-
MVSC	57.08(±9.81)	45.54(±2.03)	-	-	-	-	-
MLRSSC	31.01(±0.00)	50.14(±0.00)	30.21(±0.00)	16.92(±0.00)	-	-	-
MPAC	61.14(±0.00)	41.72(±0.00)	32.48(±0.00)	18.40(±0.00)	-	-	-
MCLES	64.47(±4.27)	46.33(±2.58)	30.47(±1.32)	-	-	-	-
FMCNOF	52.51(±4.93)	48.51(±4.22)	24.34(±2.43)	18.67(±2.38)	-	19.55(±1.86)	31.52(±2.21)
ADAGAE	-	-	-	-	-	-	-
PFSC	63.80(±6.28)	50.62(±4.77)	-	-	-	-	-
SFMC	65.88(±0.00)	50.24(±0.00)	30.17(±0.00)	15.75(±0.00)	20.53(±0.00)	22.08(±0.00)	-
MSGL	29.61(±1.03)	-	-	17.99(±0.88)	23.83(±0.64)	21.48(±0.57)	-
FPMVS	**68.46(±7.24)**	49.88(±2.19)	32.05(±1.91)	19.55(±0.19)	22.90(±2.15)	22.37(±0.62)	51.97(±3.26)
MFLVC	-	-	-	-	-	-	-
UOMVSC	66.26(±0.00)	38.84(±0.00)	30.45(±0.00)	19.29(±0.00)	26.28(±0.00)	-	-
PGSC	64.94(±7.61)	36.37(±4.52)	31.27(±2.43)	18.07(±0.74)	22.15(±0.62)	-	-
OrthNTF	-	-	-	-	-	-	-
FMVACC	-	-	-	-	-	-	-
FASTMI	64.58(±4.53)	37.46(±1.93)	34.52(±1.21)	**21.73(±0.91)**	21.79(±2.80)	23.21(±1.05)	53.12(±4.21)
Ours	66.76(±0.00)	**52.04(±0.00)**	**35.78(±0.00)**	20.06(±0.00)	**28.03(±0.00)**	**25.73(±0.00)**	**56.92(±0.00)**

clustering. To validate the effectiveness of DLA-EF-JA in gathering the information from multiple views, on the basic of Section H, we conduct clustering individually on each view of multi-view datasets mentioned earlier and compare the generated single-view clustering results and multi-view clustering results, as shown in Table 11, where V1 $\sim$ V6 denote the results based on view 1 $\sim$ 6 respectively and 'Ours' denotes the results based on all views. As seen, multi-view clustering results outperform single-view counterparts with remarkable margins in most cases, which highlights that our DLA-EF-JA is able to effectively gather multi-view information for preferable clustering. The reason of some sub-optimal results could be that the quality of certain views is relatively poor and disorganize the cluster structure.

Table 10: Single-view experimental results in Fscore

Dataset	DERMATO	CALTE7	Cora	REU7200	Reuters	CIF10Tra4	FasMNI4V
FMR	66.40(±4.64)	22.72(±0.15)	19.09(±0.23)	-	-	-	-
PMSC	68.06(±8.46)	37.68(±1.18)	27.42(±2.21)	21.34(±1.02)	-	-	-
AMGL	19.17(±0.28)	37.52(±0.89)	24.77(±0.11)	22.53(±0.00)	28.53(±0.21)	-	-
MSCIAS	67.19(±8.74)	40.65(±3.12)	23.41(±1.52)	21.07(±0.41)	30.72(±0.77)	-	-
MVSC	55.63(±10.99)	44.64(±2.87)	-	-	-	-	-
MLRSSC	33.39(±0.00)	**50.64(±0.00)**	30.40(±0.00)	23.21(±0.01)	-	-	-
MPAC	**70.02(±0.00)**	41.65(±0.00)	26.10(±0.00)	21.94(±0.00)	-	-	-
MCLES	67.27(±4.69)	48.97(±2.84)	30.34(±1.73)	-	-	-	-
FMCNOF	46.98(±3.78)	46.35(±4.21)	20.05(±2.23)	21.68(±2.79)	-	17.00(±1.17)	26.54(±1.89)
ADAGAE	-	-	-	-	-	-	-
PFSC	68.99(±4.95)	48.47(±3.26)	-	-	-	-	-
SFMC	60.29(±0.00)	47.32(±0.00)	30.35(±0.00)	20.64(±0.00)	29.04(±0.00)	15.28(±0.00)	-
MSGL	31.90(±0.97)	-	-	22.48(±0.37)	28.97(±0.24)	16.14(±0.32)	-
FPMVS	68.31(±6.97)	49.97(±2.50)	26.33(±0.70)	20.33(±1.15)	31.80(±1.64)	17.54(±0.35)	45.93(±2.06)
MFLVC	-	-	-	-	-	-	-
UOMVSC	67.90(±0.00)	38.64(±0.00)	24.19(±0.00)	22.78(±0.00)	31.91(±0.00)	-	-
PGSC	63.05(±6.85)	37.62(±4.23)	25.01(±3.77)	22.53(±1.24)	32.42(±1.53)	-	-
OrthNTF	-	-	-	-	-	-	-
FMVACC	-	-	-	-	-	-	-
FASTMI	69.65(±4.79)	39.57(±1.24)	31.67(±1.50)	19.24(±1.49)	30.45(±0.71)	15.35(±0.69)	45.68(±2.35)
Ours	69.70(±0.00)	50.41(±0.00)	**32.40(±0.00)**	**25.26(±0.00)**	**35.02(±0.00)**	**17.86(±0.00)**	**49.77(±0.00)**

J Time Overhead Proportion

To further dissect the performance of the proposed DAL-EF-JA, we count the time overhead proportion of each optimization variable, as shown in Fig. 4. From these figures, we can observe that on CALTE7 and Cora datasets, $\mathbf{B}_p$ and $\mathbf{T}_p$ occupy most of the overall optimization time, which is mainly because the number of clusters is slightly larger and accordingly the traversal searching and QCQP searching

Table 11: Effectiveness in gathering multi-view information

Dataset	Metric	Clustering Results						
		V1	V2	V3	V4	V5	V6	Ours
DERMATO	NMI	56.66	80.52					**89.97**
	ACC	60.06	66.76					**85.47**
	Fscore	49.99	69.70					**87.92**
CALTE7	NMI	17.84	36.59	34.14	**48.75**	41.74	39.98	45.25
	ACC	35.01	52.04	48.71	53.87	39.42	46.40	**80.66**
	Fscore	33.35	50.41	47.41	53.85	48.15	47.42	**78.12**
Cora	NMI	10.22	10.04	12.24	11.49			**43.70**
	ACC	30.24	35.78	30.17	29.73			**52.44**
	Fscore	30.39	32.40	30.36	29.91			**41.12**
REU7200	NMI	1.27	2.50	4.81	1.39	1.40		**6.25**
	ACC	21.24	20.06	24.06	19.61	20.83		**26.22**
	Fscore	23.67	25.26	25.41	27.01	24.90		**28.55**
Reuters	NMI	23.47	1.37	1.10	1.06	20.83		**31.87**
	ACC	46.65	28.03	27.24	27.80	47.62		**54.26**
	Fscore	42.71	35.02	35.24	35.16	43.67		**44.84**
CIF10Tra4	NMI	10.01	15.09	12.35	12.50			**15.64**
	ACC	21.89	25.73	23.25	22.05			**26.83**
	Fscore	16.46	17.86	15.87	16.34			**20.64**
FasMNI4V	NMI	49.81	**61.44**	53.26	54.86			59.21
	ACC	41.76	56.92	46.71	52.32			**57.36**
	Fscore	37.26	49.77	42.80	45.04			**51.37**

consume relatively more time than other parts. On REU7200 and Reuters, the time overhead of $\mathbf{C}$ and $\boldsymbol{\alpha}$ holds a dominant position, possibly because the higher data dimension exacerbates the computing burden of $\mathbf{W}$, $\mathbf{Z}$ and the coefficient b_p. When dealing with CIF10Tra4 and FasMNI4V, the time overhead of updating $\mathbf{T}_p$ and $\mathbf{C}$ is larger than that of other variables. Possible reasons are that the cluster number and the feature dimension on these two datasets are relatively larger and accordingly induces much time overhead. Especially, $\mathbf{T}_p$ takes the most time expenditures, which

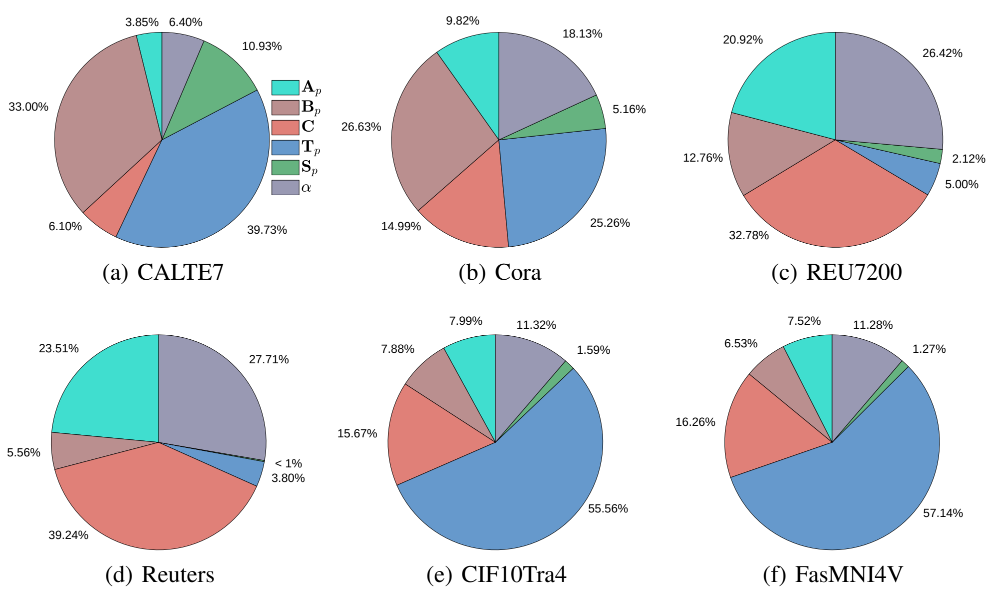

Figure 4: The time overhead proportion of different optimization variables.

is mainly due to the searching on a set of one-hot vectors. Although the time overhead proportion between optimization variables is diverse in different cases, combined with Fig. 2 we have that the overall time overhead of our DAL-EF-JA is competitive.

K CONVERGENCE

Besides owing linear complexities, our DLA-EF-JA is also convergent. To demonstrate this point, we plot the changes in function loss with respective to the number of iterations, as shown in Fig. 5. As seen, the function loss is monotonically reducing after iterations and gradually reaches to a steady state, which gives evidence that our DLA-EF-JA is convergent.

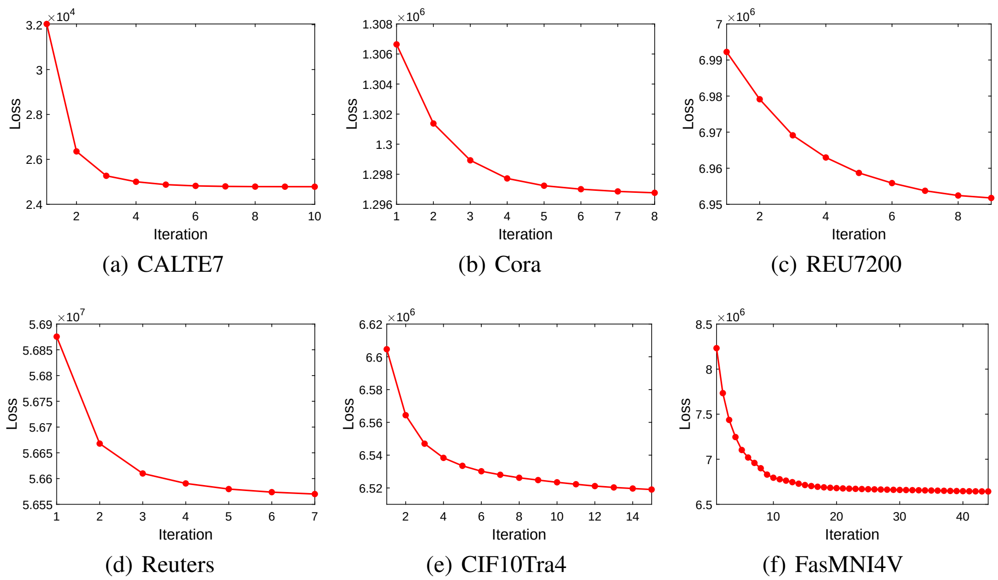

(a) CALTE7 (b) Cora (c) REU7200

(d) Reuters (e) CIF10Tra4 (f) FasMNI4V

Figure 5: The changes in function loss.

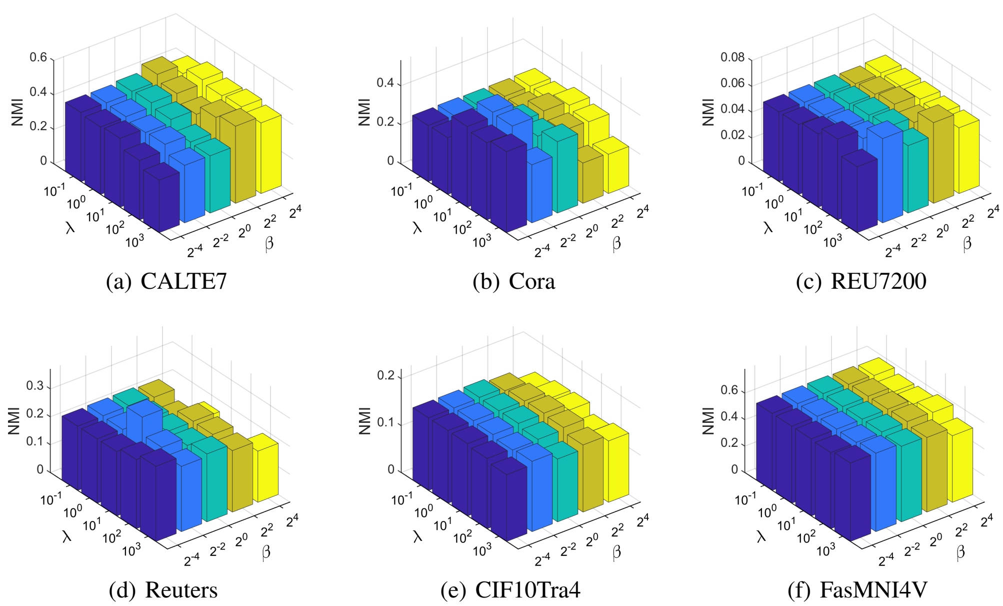

(a) CALTE7 (b) Cora (c) REU7200

(d) Reuters (e) CIF10Tra4 (f) FasMNI4V

Figure 6: Sensitivity of the parameters λ and β in terms of NMI.

L SENSITIVITY

In our DLA-EF-JA method, there involve hyper-parameters λ and β. We conduct fine tuning for them in $[10^{-1}, 10^{0}, \cdots, 10^{3}]$ and $[2^{-4}, 2^{-2}, \cdots, 2^{4}]$ respectively. To investigate the sensitivity of hyper-parameters λ and β, we plot the clustering results under each parameter combination, as shown in Fig. 6, 7 and 8. It is easy to see that with given β, the clustering results are not dramatically changed in most cases. So, we can conclude that the proposed DLA-EF-JA is not fairly sensitive to λ. Moreover, combined with Table 1, we have that within a broad range of parameters, the generated clustering results are still comparable. Thus, we can summarize that our proposed DLA-EF-JA is somewhat robust to hyper-parameters.

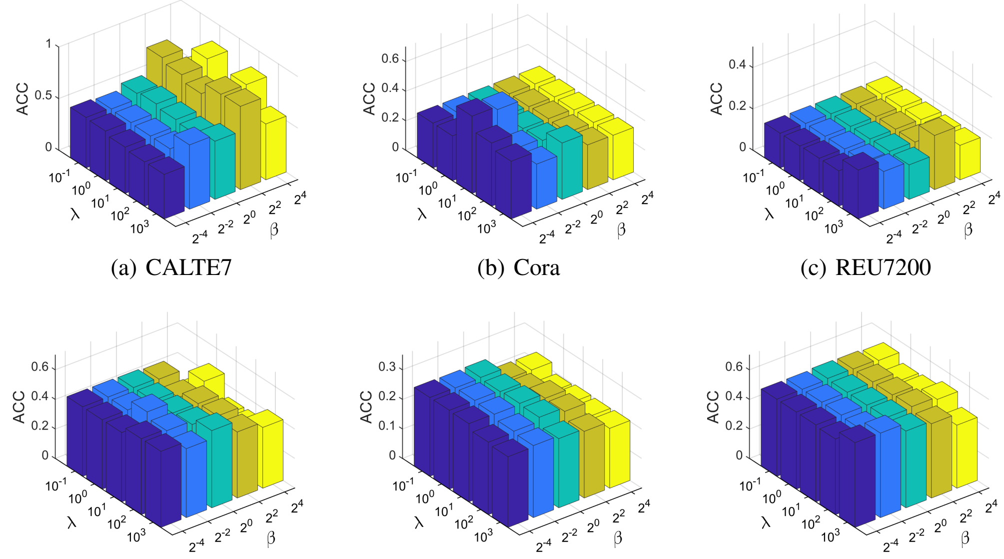

(a) CALTE7 (b) Cora (c) REU7200

(d) Reuters (e) CIF10Tra4 (f) FasMNI4V

Figure 7: Sensitivity of the parameters λ and β in terms of ACC.

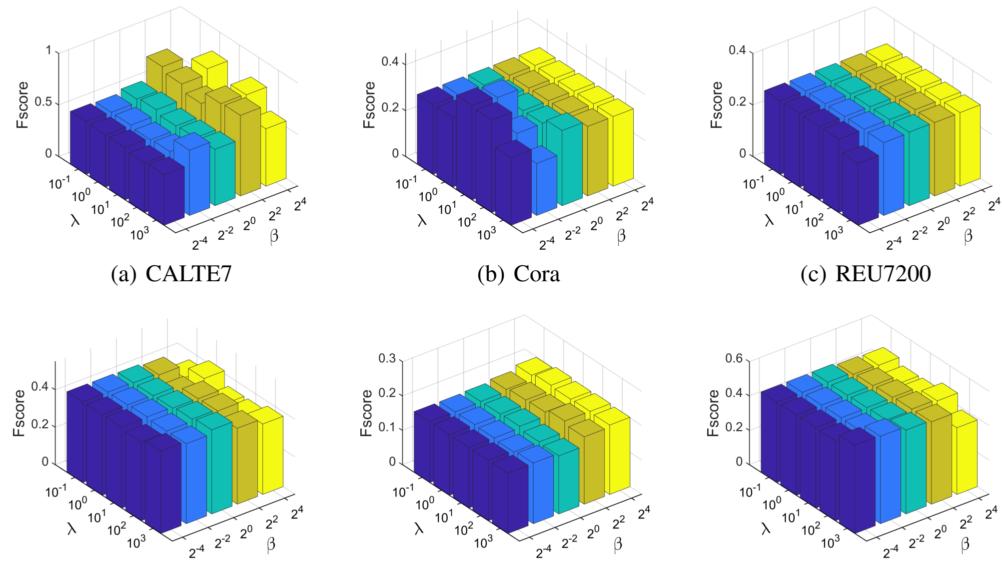

(a) CALTE7 (b) Cora (c) REU7200

(d) Reuters (e) CIF10Tra4 (f) FasMNI4V

Figure 8: Sensitivity of the parameters λ and β in terms of Fscore.

M Potential Improvement Directions

In this work, we generate anchors via learning strategy, nevertheless, we do not explicitly consider the spatial distribution of anchors. Given the fact that the role of anchors aims at approximately characterizing the overall samples, generating the anchors that are with similar distributions to original data could further enhance the clustering performance. Besides, it needs to perform searching on one-hot vectors when updating the permutation model, which could bring additional computing overhead, and thus designing other talented solutions will further accelerate its running speed.